

SHASAM: Submodular Hard Sample Mining for Fair Facial Attribute Recognition

Anay Majee
 The University of Texas at Dallas
 anay.majee@utdallas.edu

Rishabh Iyer
 The University of Texas at Dallas
 rishabh.iyer@utdallas.edu

Abstract

Deep neural networks often inherit social and demographic biases from annotated data during model training, leading to unfair predictions, especially in the presence of sensitive attributes like race, age, gender etc. Existing methods fall prey to the inherent data imbalance between attribute groups and inadvertently emphasize on sensitive attributes, worsening unfairness and performance. To surmount these challenges, we propose **SHASAM** (**S**ubmodular **H**ard **S**ample **M**ining), a novel combinatorial approach that models fairness-driven representation learning as a submodular hard-sample mining problem. Our two-stage approach comprises of SHASAM-MINE, which introduces a submodular subset selection strategy to mine hard positives and negatives — effectively mitigating data imbalance, and SHASAM-LEARN, which introduces a family of combinatorial loss functions based on Submodular Conditional Mutual Information to maximize the decision boundary between target classes while minimizing the influence of sensitive attributes. This unified formulation restricts the model from learning features tied to sensitive attributes, significantly enhancing fairness without sacrificing performance. Experiments on CelebA and UTKFace demonstrate that SHASAM achieves state-of-the-art results, with up to 2.7 points improvement in model fairness (Equalized Odds) and a 3.5% gain in Accuracy, within fewer epochs as compared to existing methods.

1. Introduction

Training modern Deep Neural Networks (DNNs) [11, 18] on curated datasets often incorporates the social and demographic biases of human annotators, which can result in unfair predictions during inference. While removing these biases is challenging as they reflect real-world scenarios, various approaches aim to mitigate their impact by encouraging DNNs to learn fair feature representations. Contrastive learning [5, 19, 31] methods, for example,

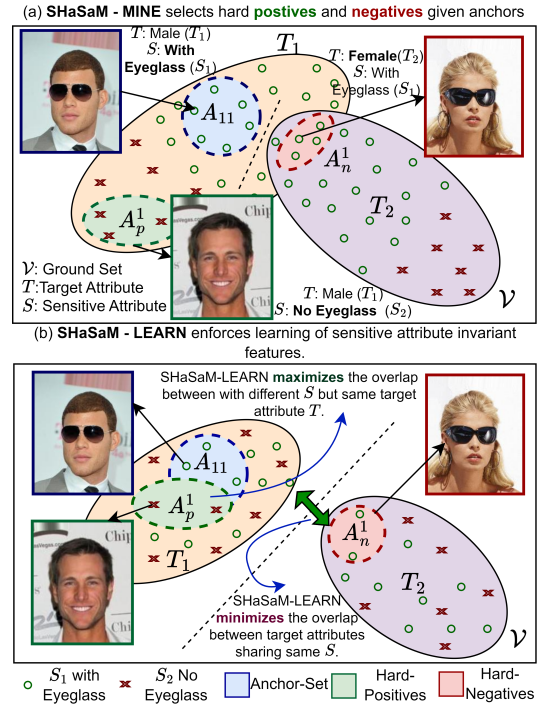


Figure 1. **Illustration of SHASAM** - Given a target T (gender) and sensitive attribute S (eyeglasses) set, (a) SHASAM-MINE selects hard-positives A_p^1 and hard-negatives A_n^1 given anchor set A_{11} . (b) SHASAM-LEARN enforces a decision boundary between target attributes T invariant to the sensitive attribute S .

have been applied to group instances with similar target attributes and separate those with different attributes to enhance fairness. However, these approaches could induce biased responses [48, 58] in the presence of sensitive attributes like race, age, gender etc. Park et al. [48] attributes this to the inadvertent learning of irrelevant features linked to sensitive attributes, weakening the decision boundary between target attributes and impacting fairness in downstream tasks. Additionally, real-world datasets [38, 40, 69] often exhibit significant imbalances in target and sensitive attributes due to the curation process, introducing biases that favor more abundant attributes and

exacerbate unfair predictions. While imbalance among attribute groups has been addressed in tasks like image recognition [8, 12, 42], imbalances in sensitive attributes have received limited attention, despite introducing high intra-group variance [48] within each target class and ultimately degrading downstream performance.

To address challenges in fair facial attribute recognition, we propose **SHASAM**, a combinatorial (set-based) method that frames fairness-driven representation learning as a Submodular Hard Sample Mining task. Motivated by the recent success of [42, 43] in introducing combinatorial objectives for representation learning, *we introduce a set-based (combinatorial) viewpoint in facial attribute recognition* (see Sec. 3.1) allowing us to leverage the benefits of submodular functions [15] to learn target attribute representations invariant to the sensitive ones. At first, SHASAM-MINE selects hard-positives and hard-negatives for each diverse set of anchor examples (all with the same target and sensitive attribute) as shown in Fig. 1(a), modeling hard-sample mining as a combinatorial selection problem [27, 35, 39]. Following the intuition in Park et al. [48], SHASAM-MINE mines hard-positives with the same target but different sensitive attributes and hard-negatives with the same sensitive but different target attributes, thus **balancing positives and negatives per training iteration to mitigate attribute group imbalances**.

Finally, SHASAM-LEARN introduces a family of objectives based on Submodular Conditional Mutual Information (CMI) [36]. Minimizing CMI in SHASAM-LEARN leverages the diversity-maximizing [39] and cooperation-enhancing [24] properties of submodular functions in a unified objective. As shown in Fig. 1(b), we simultaneously maximize the information overlap between anchors and hard-positives and minimizes inter-group separation between anchors and hard-negatives mined by SHASAM-MINE. This unified framework **restricts the model from learning features linked to sensitive attributes, significantly enhancing fairness** without sacrificing downstream performance. In practice, SHASAM-MINE and SHASAM-LEARN are sequentially invoked at each training iteration on the facial attribute recognition benchmarks [48, 63] demonstrating the following major contributions:

- **SHASAM introduces a novel set-based combinatorial viewpoint in fair facial attribute classification** by modeling fair attribute recognition as a **submodular hard-sample mining problem** using a two-stage framework encouraging the learning of fair feature embeddings corresponding to target attributes without biasing on sensitive ones during model training.
- Components of SHASAM, namely SHASAM-MINE **employs a novel submodular subset selection strategy** to mine hard-positives and hard-negatives mitigating the impedance of *data imbalance among attribute groups*

(detailed in Sec. 3.4).

- **SHASAM-LEARN introduces a family of combinatorial objectives based on Submodular Conditional Mutual Information which presents an unified approach to improve fairness** in model predictions by minimizing the information overlap between target classes sharing the same sensitive attribute while maximizing the overlap within target classes sharing different sensitive attributes.
- Overall, SHASAM demonstrates up to **2.7 points improvement in fairness metrics (quantified through Equalized Odds (EO))**, achieving up to 3.5% boost in Top-1 Acc. on popular facial attribute recognition benchmarks like CelebA and UTKFace within fewer training epochs.

2. Related Work

Ensuring fairness in machine learning, particularly in facial attribute classification, has become pivotal due to the significant progress has been made in mitigating biases while maintaining high model performance. Early efforts focused on adversarial learning and dataset adjustments. Wadsworth et al. [64] pioneered adversarial learning to reduce bias in decision-making tasks, while Raff and Sylvester [51] proposed gradient reversal techniques to mitigate discrimination in neural networks; both demonstrated the effectiveness of adversarial approaches during training. To address gender bias in facial recognition, Zhao et al. [70] proposed a debiasing technique that generates gender-neutral face embeddings, significantly improving fairness. Similarly, Kim et al. [34] introduced an adversarial framework to prevent models from learning biased data representations. Disentanglement methods were also explored, with Creager et al. [7] separating sensitive and non-sensitive features in learned representations, and Arjovsky et al. [1] introducing Invariant Risk Minimization (IRM) to learn representations invariant to data distribution shifts. Dataset balancing methods have been adopted to mitigate attribute imbalance and reduce inter-attribute bias [38, 51, 55]. FairFace [38] introduced a dataset designed to address imbalances in race, gender, and age within facial attribute classification tasks. Techniques like gradient reversal [51] and resampling of rare attributes [55] achieve lower equalized odds, ensuring equitable outcomes across diverse demographic groups.

Generative models have also played a prominent role in promoting fairness. Shen et al. [59] introduced InterfaceGAN, leveraging Generative Adversarial Networks (GANs) to manipulate latent space representations of facial attributes such as age and gender, allowing fine-tuned control over fairness in attribute manipulation tasks. Orthogonal disentanglement between task-specific and sensitive attributes, as shown by Sarhan et al. [56], improved fairness across downstream classification tasks. Additionally, Wang et al. [67] explored various strategies for bias

mitigation in visual recognition, including resampling and re-weighting techniques, contributing significantly toward mitigating bias in large-scale vision systems.

Recent advancements in fairness-aware representation learning have focused heavily on contrastive learning [5, 6, 19, 31]. Park et al. [47] proposed a fairness-aware information alignment method to disentangle sensitive attributes, enhancing fairness in facial attribute classification. Ramaswamy et al. [52] applied latent space debiasing techniques to eliminate correlations between target outputs and sensitive features without sacrificing accuracy. Jung et al. [25] introduced Fair Feature Distillation, a contrastive learning method aimed at learning invariant representations, further enhancing fairness in visual recognition. Latent space smoothing, proposed by Peychey et al. [49], ensures that small input variations do not lead to disproportionately large changes in model predictions. This approach, along with fairness-preserving latent representations in Roh et al. [54], balances fairness and model performance. Transformer-based methods have also been explored; Qiang et al. [50] and Sudhakar et al. [62] introduced Debiased Self-Attention and TADeT, respectively, aiming to eliminate biases in Vision Transformers. More fundamentally, Tian et al. [63] modified the attention head architecture in Vision Transformers [10] to induce fairness. Although transformer-based approaches improve both fairness and performance, they come with significant computational overhead.

Representation learning techniques have thus shown remarkable promise in addressing the fairness challenges inherent in facial attribute classification. From early disentanglement methods [7] to recent advancements in contrastive learning [25, 48, 58] and latent space smoothing [49], these techniques have transformed how fairness is incorporated into facial recognition models. Fair representation learning has evolved into a comprehensive field where sensitive attributes are decoupled from task-specific features, ensuring unbiased predictions while retaining strong performance. As demonstrated by Madras et al. [41], adversarial learning can be effectively applied to achieve fair and transferable representations, laying the foundation for future work in this critical area. Shen et al. [58] further advanced this field by incorporating contrastive learning approaches that significantly reduce bias in large-scale visual systems, solidifying the role of representation learning as a cornerstone in building equitable Artificial Intelligence (AI) systems.

3. Method

3.1. Problem Definition

We consider a dataset $D \in D^{train} \cup D^{test}$ with a training set D^{train} consisting of N labeled samples such that $\{x_i, t_i, s_i\}_{i=1}^N$. Here, x_i represents the raw data

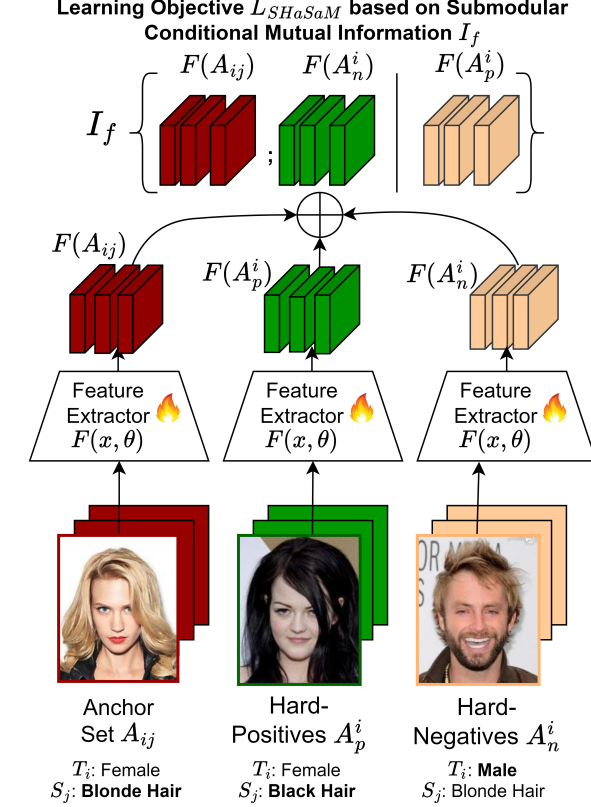


Figure 2. **Training Strategy in SHASAM-LEARN** which learns parameters of $F(x, \theta)$ by minimizing a novel combinatorial objective L_{SHASAM} to learn features invariant to sensitive attributes.

while t_i and s_i jointly compose the label indicating the target and sensitive attribute for x_i in D^{train} . Introducing a combinatorial viewpoint as in [42, 43] we formulate D_{train} as a collection of sets (each containing a set of datapoints) based on the target attribute T_i or the sensitive attribute S_i such that $D_{train} = \mathcal{V} = \cup_{i=1}^N T_i = \cup_{j=1}^K S_j$, where $N \neq K$. A feature extractor $F(A; \theta)$, maps all instances in the input set A into a lower dimensional feature space and a classifier $Clf(F(A); \theta)$ maps the learnt feature representations to its corresponding target attribute $i \in N$ irrespective of the sensitive attribute $j \in K$. The optimization task [48, 58] is to maximize the probability of all elements in A belonging to the target class T_i without biasing on the sensitive attribute S_j .

3.2. Preliminaries: Submodularity

Submodular functions [4, 15, 20] are set functions characterized by a natural diminishing returns property. Specifically, a set function $f : 2^{\mathcal{V}} \rightarrow \mathbb{R}$, defined over a ground set \mathcal{V} , is submodular if it satisfies the inequality $f(A_i) + f(A_j) \geq f(A_i \cup A_j) + f(A_i \cap A_j)$ for all subsets $A_i, A_j \subseteq \mathcal{V}$ [15]. These functions have been extensively researched in areas such as data subset selection [13, 23, 32, 33, 36], active learning [3, 28, 35, 68], and video summariza-

tion [27, 29, 30]. Traditionally, subset selection and summarization tasks are modeled as a discrete optimization problem through submodular maximization [15, 45] under a knapsack constraint [45]. This can be fairly approximated with a $(1 - e^{-1})$ constant factor guarantee [45] using greedy optimization techniques [44, 45]. Maximizing **Submodular Information Functions** (SIMs) [4, 21, 22] $f(A)$ like Facility-Location, Graph-Cut etc. promotes selection of diverse examples within a set A , while maximizing **Submodular Mutual Information Functions** (SMIs) $I_f(A; Q)$ selects examples that share maximum information in $A \cap Q$. Complimentary to SMI, **Submodular Conditional Gain** (SCG) $H_f(A|Q)$ selects examples in A with maximum dissimilarity to Q , while **Submodular Conditional Mutual Information** (SCMI) $I_f(A; Q|P)$ selects examples in A similar to Q but dissimilar to P . Here, P and Q are disjoint sets. We include more details in the Appendix. Interestingly, recent approaches [42, 43] have also applied combinatorial functions as learning objectives in continuous optimization problems. Specifically, Majee et al. [42] introduces combinatorially inspired loss functions (in this case SIMs) which model intra-group compactness (cooperation) when minimized and inter-group separation when maximized. Additionally, [43] introduces SMI as loss function to model interactions between abundant and rare examples in data-efficient (few-shot) representation learning tasks. In our paper, we exploit a mixture of discrete and continuous optimization tasks through a novel combinatorial approach to induce fairness in representation learning.

3.3. SHASAM: Submodular Hard Sample Mining

Existing works in fair attribute recognition (refer Sec. 2) highlight two major challenges in the domain - (1) Overcoming large *imbalance* not only between target attributes but also between sensitive attributes (with the same target attribute), and (2) Learning discriminative *feature representations* for each target attribute $T_i \in \mathcal{V}$ without biasing on the sensitive attribute $S_j \in \mathcal{V}$. In a quest to learn a target attribute T_i , examples with rare sensitive attributes S_j belonging to T_i act as hard positives while examples belonging to $\mathcal{V} \setminus T_i$ (with the same S_j) act as hard negatives [61].

In this paper, we introduce a novel unified approach SHASAM by modeling fairness driven representation learning as a combinatorial hard sample mining problem. We achieve this through two key steps - (1) **SHASAM-MINE** (detailed in Sec. 3.4) which mines hard positives A_p^i and hard negatives A_n^i given a anchor set A_{ij} mined from the dataset \mathcal{V} , and (2) **SHASAM-LEARN** (detailed in Sec. 3.5) which introduces a family of novel combinatorial learning objectives based on Submodular Conditional Mutual Information to jointly maximizes cluster overlap between A_{ij} and A_p^i (which share different S_j 's) while maximizing the decision boundary between A_{ij} and A_n^i (which share the

same S_j but belong to different T_i 's).

We define the selection of a candidate set A from a collection Q as a softmax over a selection function \mathcal{F} as shown in Eq. (1). This definition of softmax serves as an approximation of the indicator over the argmax function. This is a smooth approximation modeling the selection of the most relevant example (positive / negative) from Q depending on the choice of \mathcal{F} similar to the definition in Song et al. [61].

$$\text{softmax}(\mathcal{F}(\cdot), A, Q) = \frac{e^{\mathcal{F}(A)}}{\sum_{p \in Q} e^{\mathcal{F}(p)}} \approx \mathbb{1}_{\underset{A \subseteq Q}{\text{argmax}} \mathcal{F}(A)} \quad (1)$$

Now, given a diverse set of anchors $A_{ij} \in \{T_i \cap S_j\}, \forall i, j \in |\mathcal{V}|, T_i \cap S_j \neq \emptyset$, we mine hard-positives A_p^i from $T_i \cap \overline{S_j}$ which maximizes the Submodular Conditional Gain (SCG) $H_f(\cdot | A_{ij})$ denoted as $\text{softmax}(H_f(\cdot | A_{ij}), A_p^i, T_i \cap \overline{S_j})$. Similarly, we mine hard-negatives A_n^i from $\mathcal{V} \setminus T_i \cap S_j$ which maximizes the Submodular Mutual Information (SMI) $I_f(\cdot; A_{ij})$ denoted as $\text{softmax}(I_f(\cdot; A_{ij}), A_n^i, \mathcal{V} \setminus T_i \cap S_j)$. Here, I_f and H_f act as selection functions. The mined anchors, hard-positives and hard-negatives mined at each training iteration train the parameters of the feature extractor $F(\cdot; \theta)$ by minimizing a novel combinatorial learning objective $L_{\text{SHASAM}}(A_{ij}, A_p^i, A_n^i; \theta)$ defined in SHASAM-LEARN (refer Sec. 3.5). Jointly, we can thus summarize the hard-sample sample mining task as a joint selection and representation learning problem described in Eq. (8).

$$\begin{aligned} L_{\text{SHASAM}}(\theta) = & \sum_{\forall i, j \in |\mathcal{V}|} \underbrace{\text{softmax}(H_f(\cdot | A_{ij}), A_p^i, T_i \cap \overline{S_j})}_{\text{(A) Selecting Hard Positives in } T_i \cap \overline{S_j}} \\ & \times \underbrace{\text{softmax}(I_f(\cdot; A_{ij}), A_n^i, \mathcal{V} \setminus T_i \cap S_j)}_{\text{(B) Selecting Hard Negatives in } \mathcal{V} \setminus T_i \cap S_j} \\ & \times \underbrace{L_{\text{SHASAM}}(A_{ij}, A_p^i, A_n^i; \theta)}_{\text{(C) SHASAM-LEARN}} \end{aligned} \quad (2)$$

We minimize $L_{\text{SHASAM}}(\theta)$ during model training. Note that $L_{\text{SHASAM}}(\theta) \approx L_{\text{SHASAM}}(\hat{A}_{ij}, \hat{A}_p^i, \hat{A}_n^i; \theta)$ where $\hat{A}_p^i = \text{argmax}_{A \subseteq T_i \cap \overline{S_j}} H_f(A | A_{ij})$ and $\hat{A}_n^i = \text{argmax}_{A \subseteq \mathcal{V} \setminus T_i \cap S_j} I_f(A; A_{ij})$. Similarly, $\nabla L_{\text{SHASAM}}(\theta) \approx \nabla L_{\text{SHASAM}}(\hat{A}_{ij}, \hat{A}_p^i, \hat{A}_n^i; \theta)$ since the gradients of the other terms involving the softmax is close to 0. This reduces the learning problem to minimizing L_{SHASAM} on the mined anchors, hard positives and negatives as shown in Fig. 2. The aforementioned phenomenon further enables us to model the selection functions in (A) and (B) as submodular maximization [15, 45] tasks, $\text{argmax}_{A \subseteq Q, |A| \leq k} \mathcal{F}(A)$, under a cardinality constraint

$|A| \leq k$ (selecting k examples in A), given \mathcal{F} is inherently submodular. This is further described in Sec. 3.4.

3.4. SHASAM-MINE

Given the ground set \mathcal{V} (as defined in Sec. 3.1) and a budget k we select anchors, hard positives and negatives through a novel selection strategy SHASAM-MINE as elucidated in Algorithm 1. For every iteration t in an epoch we choose candidate target and sensitive attributes i and j (lines 16, 17 in Algorithm 1), $\forall i, j \in |\mathcal{V}|$ such that samples in $T_i \cap S_j \neq \emptyset$. Next, we mine anchor set A_{ij} for the selected (T_i, S_j) pair through submodular maximization of the Log-Determinant (LogDet) function $f(A_{ij})$ over each subset $A_{ij} \in \mathcal{V}$ as shown in line 19 of Algorithm 1, under a cardinality constraint. Fig. 4(a) shows that maximizing LogDet selects diverse examples [27] from $T_i \cap S_j$ in A_{ij} . Following this step, we perform a two stage selection on \mathcal{V} to identify hard-positives A_p^i and hard-negatives A_n^i relative to the choice of a diverse anchor set A_{ij} .

Hard-Positive samples A_p^i are selected by *maximizing the SCG function $H_f(A_p^i | A_{ij})$ over all samples in $T_i \cap \overline{S_j}$* to mine exactly k (represented as *budget*) as shown in line 20 of Algorithm 1. Maximizing SCG results in selection of samples which have maximum dissimilarity to the ones in A_{ij} [36] but share the same T_i . Following Kothawade et al. [36], we adopt the Facility Location (FL) as the underlying function to compute the SCG resulting in selection of representative *hard-positives* in A_p^i (share the same class label but different sensitive attribute with A_{ij}) located at the cluster boundary of T_i as shown in Fig. 4(b).

Hard-Negative samples in $A_n^i \subseteq \mathcal{V} \setminus T_i \cap S_j$ are selected such that it *maximizes the SMI function $I_f(A_n^i; A_{ij})$ between the anchor set A_{ij} and A_n^i* as shown in line 21 of Algorithm 1 under the same cardinality constraint. Adopting Facility-Location as the underlying submodular function, the resultant subset A_n^i upon maximizing SMI contains examples most similar to A_{ij} [26, 36], sharing the same sensitive attribute label S_j but with a different target attribute from the samples in A_{ij} .

Note that all maximization steps follow discrete optimization through the Lazy-Greedy algorithm [44] (detailed in Appendix) under a cardinality constraint (same across tasks). Interestingly, application of the cardinality constraint results in balanced selection $|A_{ij}| = |A_p^i| = |A_n^i| = k$ in each input batch, *significantly overcoming the effect of class-imbalance between attribute groups*.

3.5. SHASAM-LEARN

Given a ground set \mathcal{V} (as defined in Sec. 3.1), a submodular function $f(A, \theta)$ over a set A and an input batch of examples from SHASAM-MINE $\{A_{ij}, A_p^i, A_n^i\}$ at each iteration, we define a loss function $L_{\text{SHASAM}}(\theta)$ in SHASAM-LEARN (refer Algorithm 1) as an instance of

Algorithm 1 Representation Learning stage in SHASAM

Require: Dataset D^{train} , Model F , Initialized model parameters θ , No. of epochs E , Batch size b , budget k

- 1: */** Training Loop in SHASAM */*
- 2: $\mathcal{V}_{\text{prev}} = \emptyset$
- 3: **for** $e = 1, 2, \dots, E$ **do**
- 4: $\mathcal{V} \leftarrow \text{RANDOM-SAMPLE}(D^{\text{train}}, 0.2) \setminus \mathcal{V}_{\text{prev}}$
- 5: **for** $t = 1, 2, \dots, |\mathcal{V}|/b$ **do**
- 6: $\{A, P, N\} = \text{SHASAM-MINE}(\mathcal{V}, k)$
- 7: */* Forward pass */*
- 8: $h_A, h_P, h_N \leftarrow F(A; \theta), F(P; \theta), F(N; \theta)$
- 9: $L(\theta), \nabla_{\theta} \leftarrow \text{SHASAM-LEARN}(h_A, h_P, h_N, \theta)$
- 10: $\theta := \theta - \eta \cdot \nabla_{\theta}$ *>// Backward Pass*
- 11: **end for**
- 12: $\mathcal{V}_{\text{prev}} = \mathcal{V}$
- 13: **end for**
- 14: */** Hard Sample Mining in SHASAM-MINE */*
- 15: **function** SHASAM-MINE(\mathcal{V}, k)
- 16: $i = \text{RANDOM-CHOICE}([1, |\mathcal{V}|])$
- 17: $j = \text{RANDOM-CHOICE}([1, |\mathcal{V}|])$
- 18: **Assert** $T_i \cap S_j \neq \emptyset$
- 19: $A_{ij} \leftarrow \underset{A_{ij} \in T_i \cap S_j, |A_{ij}| \leq k}{\text{argmax}} f(A_{ij})$
- 20: $A_p^i \leftarrow \underset{A_p^i \subseteq T_i \cap \overline{S_j}, |A_p^i| \leq k}{\text{argmax}} H_f(A_p^i | A_{ij})$
- 21: $A_n^i \leftarrow \underset{A_n^i \subseteq \mathcal{V} \setminus T_i \cap S_j, |A_n^i| \leq k}{\text{argmax}} I_f(A_n^i; A_{ij})$
- 22: **return** $\{A_{ij}, A_p^i, A_n^i\}$
- 23: **end function**
- 24: */** Learning Objective in SHASAM-LEARN */*
- 25: **function** SHASAM-LEARN($\hat{A}_{ij}, \hat{A}_p^i, \hat{A}_n^i, \theta$)
- 26: $L_{\text{SHASAM}}(\theta) = \frac{1}{N_f(\hat{A}_{ij})} I_f(\hat{A}_{ij}; \hat{A}_n^i | \hat{A}_p^i; \theta)$
- 27: $\nabla L_{\text{SHASAM}}(\theta) = \nabla L_{\text{SHASAM}}(\hat{A}_{ij}, \hat{A}_p^i, \hat{A}_n^i; \theta)$
- 28: **return** $L_{\text{SHASAM}}(\theta), \nabla L_{\text{SHASAM}}(\theta)$
- 29: **end function**

Submodular Conditional Mutual Information (SCMI) function $I_f(A_{ij}; A_n^i | A_p^i, \theta) = f(A_{ij} \cup A_p^i) + f(A_n^i \cup A_p^i) - f(A_{ij} \cup A_p^i \cup A_n^i) - f(A_p^i)$ which jointly minimizes the feature overlap between A_{ij} and A_n^i while maximizing the mutual information between A_{ij} and the hard-positives A_p^i as shown in Eq. (3). Here, $N_f(A_{ij})$ is the normalization constant.

$$L_{\text{SHASAM}}(\theta) = \sum_{\forall i, j \in |\mathcal{V}|} \frac{1}{N_f(A_{ij})} I_f(A_{ij}; A_n^i | A_p^i; \theta) \quad (3)$$

This formulation largely differs from [42, 43] which introduce combinatorial objectives to model either intra-group compactness through SIMs [42] or inter-group separation through SMI [43] without unifying these properties into a single formulation as shown in SHASAM. Further, Sec. 3.4

Table 1. **Instances of learning objectives in SHASAM-LEARN** obtained by varying the submodular function $f(A)$ over a set A . Here S indicates the cosine similarity kernel.

| Instance Name | $L_{\text{SHASAM}}(A_{ij}, A_p^i, A_n^i, \theta)$ |
|------------------|--|
| SHASAM-FLCMI | $\sum_{i,j \in \mathcal{V} } \frac{1}{3 A_{ij} } \left(\max \left(\min \left(\max_{a \in A_{ij}} S_{ia}, \max_{n \in A_n^i} S_{in} \right) - \max_{p \in A_p^i} S_{ip}, 0 \right) \right)$ |
| SHASAM-LogDetCMI | $\sum_{i,j \in \mathcal{V} } \frac{1}{3 A_{ij} } \log \frac{\det(I - S_{A_p^i}^{-1} S_{A_{ij}, A_p^i} S_{A_p^i}^{-1} S_{A_n^i, A_p^i}^T)}{\det(I - S_{A_{ij} \cup A_p^i}^{-1} S_{A_{ij} \cup A_p^i, A_n^i} S_{A_n^i}^{-1} S_{A_{ij} \cup A_p^i, A_n^i}^T)}$ |

points out that A_p^i and A_n^i are located at the cluster boundary of disjoint feature clusters. Thus, minimizing L_{SHASAM} increases the decision boundary between them. Concurrently, minimizing L_{SHASAM} enforces an increased feature overlap between A_{ij} and A_p^i which belong to the same T_i but differ in the sensitive attribute label S_j . This results in a *compact feature cluster for T_i invariant to the sensitive attribute enforcing fairness* in the learning process.

We model interactions between samples within/across sets using the cosine similarity kernel $S_{ij}(\theta) = \frac{F(x_i, \theta)^T \cdot F(x_j, \theta)}{\|F(x_i, \theta)\| \cdot \|F(x_j, \theta)\|}$, $\forall i, j \in |\mathcal{V}|$ and aggregate these interactions to compute the SCMI objective. By varying the submodular function $f(A, \theta)$ between Facility-Location (FL) and LogDet we introduce a family of objectives - SHASAM-FLCMI and SHASAM-LogDetCMI summarized in Tab. 1 with detailed derivations in the Appendix. Empirical evidence in Sec. 4 suggest that SHASAM-FLCMI based objective outperforms other instances alongside SoTA approaches in fair attribute classification due to its inherent self-balancing [42] property alongside being insensitive to the presence of sensitive attributes during training.

4. Experiments

Datasets We perform our experiments on two benchmark datasets adopted from [48, 58, 63] -

(1) **CelebA** [40] contains approximately 200k facial images annotated with 40 binary attributes. We follow [48] and designate 'male' (m) and 'young' (y) as the sensitive attributes and select target attributes that exhibit the highest Pearson correlation with these sensitive attributes. To ensure reliable evaluation, we manually exclude attributes that are extremely correlated; for instance, the 'heavy-makeup' attribute. Consequently, we utilize three single target attributes: 'attractiveness' (a), 'big nose' (b), and 'bags under eyes' (e), as well as a pair of target attributes - 'big nose', 'bags under eyes'.

(2) **UTKFace dataset** [69] comprises about 20,000 facial images with annotations for gender, age, and ethnicity. We set 'age' and 'ethnicity' as sensitive attributes and 'gender' as the target attribute. We transform 'age' and 'ethnicity' into binary attributes based on whether the age is under

35 or not, and whether the ethnicity is Caucasian or not, respectively [48, 58]. In our constructed datasets, one sensitive group (e.g., Caucasian) contains α times more male data than female data, while the other sensitive group has the opposite gender ratio. We set α to 2, 3, and 4 to simulate different levels of bias. Unlike the training set, we organize completely balanced validation and test sets to ensure fair evaluation.

Experimental Setup We adopt a two-stage training strategy [31, 48] to train the feature extractor F and the classifier Clf in SHASAM. We follow Park et al. [48] and choose a ResNet-18 [18] based architecture for F and a vision-transformer based architecture [11] for contrasting against FairViT [63]. Following the augmentation strategy described in [31], we generate two cropped patches per image in the dataset and resize them to 128×128 pixels to feed as input to F . We train the encoder networks for 20 epochs during the representation learning phase (stage 1) optimized through L_{SHASAM} with a set batch size to 96 (16 anchors, 16 positives and 16 negatives in each iteration with 2 augmentations per image), an initial learning rate of 0.4, a cosine annealing scheduler and a temperature of 0.7. The latent space dimensions are set to 256 for the encoder and 128 for the projection network following the observations in Khosla et al. [31]. Next, we freeze the feature extractor (from stage 1) and training Clf (stage 2) with one hidden layer for 10 epochs using cross-entropy loss [2], a batch size of 128 and a constant learning rate of 0.1.

Metrics Following most works in image classification we report the Top-1 Accuracy of predicting the target attribute T . For estimating the fairness aspect of SHASAM we report the Equalized Odds (EO) [17] which focuses on both the discrepancy between the True Positive Rate (TPR) and False Positive Rate (FPR) among sensitive attribute groups.

A low value of EO indicates non-discriminative/ insensitive response of the model to the sensitive attributes indicating higher fairness in predictions. Although measures like Demographic Parity (DP) [37] and Equal Opportunity (EOpp) exists in literature but [48] points out the sensitivity to deliberate mis-classifications and discounting unfairness in negative classes as major pitfalls in DP and EOP respectively. The experimental results are aggregated over several independent runs on 4 NVIDIA A6000 GPUs with additional details in the Appendix.

4.1. Contrasting Against Baselines

We compare the performance of SHASAM against several SoTA benchmarks as baselines - vanilla CE [2], GRL [51], LNL [34], FD-VAE [47], MFD [25], FSCL [48] and FairViT [63] and report the top-1 accuracy (Acc.) and Equalized Odds (EO) in Tab. 2. Although CE, LNL and GRL improve the learning of decision boundaries between target classes in CelebA characterized by gains

Table 2. **Classification results on CelebA** measured in terms of Top-1 Accuracy (Acc.) and equalized odds (EO) by varying the target T and sensitive attributes S . Here, a , b , e , m , and y denote attractiveness, big nose, bags-under-eyes, male, and young, respectively. All results are averaged over three independent runs. * indicates our re-implementations.

| Method | $T = a / S = m$ | | $T = a / S = y$ | | $T = b / S = m$ | | $T = b / S = y$ | | $T = e / S = m$ | | $T = e / S = y$ | | $T = e \& b / S = m$ | | $T = a / S = m \& y$ | |
|----------------------------|-----------------|----------|-----------------|----------|-----------------|----------|-----------------|----------|-----------------|----------|-----------------|----------|----------------------|----------|----------------------|----------|
| | EO (↓) | Acc. (↑) | EO (↓) | Acc. (↑) | EO (↓) | Acc. (↑) |
| CE [2] | 27.8 | 79.6 | 16.8 | 79.8 | 17.6 | 84.0 | 14.7 | 84.5 | 15.0 | 83.9 | 12.7 | 83.8 | 12.9 | 72.6 | 31.3 | 79.5 |
| GRL [51] | 24.9 | 77.2 | 14.7 | 74.6 | 14.0 | 82.5 | 10.0 | 83.3 | 6.7 | 81.9 | 5.9 | 82.3 | 9.4 | 71.4 | 22.9 | 78.6 |
| LNL [34] | 21.8 | 79.9 | 13.7 | 74.3 | 10.7 | 82.3 | 6.8 | 82.3 | 5.0 | 81.6 | 3.3 | 80.3 | 7.4 | 70.8 | 20.7 | 77.7 |
| FD-VAE [47] | 15.1 | 76.9 | 14.8 | 77.5 | 11.2 | 81.6 | 6.7 | 81.7 | 5.7 | 82.6 | 6.2 | 84.0 | 8.2 | 70.2 | 19.9 | 78.0 |
| MFD [25] | 7.4 | 78.0 | 14.9 | 80.0 | 7.3 | 78.0 | 5.4 | 78.0 | 8.7 | 79.0 | 5.2 | 78.0 | 9.0 | 70.0 | 19.4 | 76.1 |
| SupCon [31] | 30.5 | 80.5 | 21.7 | 80.1 | 20.7 | 84.6 | 16.9 | 84.4 | 20.8 | 84.3 | 10.8 | 84.0 | 12.5 | 72.7 | 24.4 | 81.7 |
| FSCL (w/ group norm) [48]* | 6.5 | 79.1 | 12.4 | 79.1 | 4.7 | 82.9 | 4.8 | 84.1 | 3.0 | 83.4 | 1.6 | 83.5 | 2.5 | 70.8 | 17.0 | 77.2 |
| SHASAM(w/ LogDetCMI) | 6.1 | 80.7 | 10.5 | 78.6 | 3.6 | 84.5 | 4.2 | 85.9 | 2.7 | 85.0 | 1.7 | 84.0 | 2.5 | 71.3 | 15.8 | 78.7 |
| SHASAM(w/ FLCMI) | 5.5 | 81.3 | 9.9 | 79.6 | 3.3 | 84.7 | 3.9 | 87.0 | 2.6 | 85.8 | 1.6 | 84.4 | 2.2 | 71.8 | 14.6 | 79.5 |
| FSCL (w/ ViT) [48]* | 5.7 | 79.9 | 10.8 | 80.0 | 4.0 | 85.0 | 4.6 | 88.2 | 2.9 | 87.7 | 1.7 | 86.3 | 2.5 | 72.8 | 16.3 | 81.8 |
| TADet [62] | 7.2 | 78.8 | 11.9 | 77.4 | 3.9 | 84.3 | 5.5 | 85.4 | 3.8 | 87.5 | 2.73 | 86.0 | 2.59 | 72.8 | 17.9 | 79.9 |
| FairViT [63]* | 6.4 | 83.8 | 12.6 | 82.5 | 5.1 | 86.1 | 4.7 | 89.3 | 3.4 | 88.1 | 1.8 | 86.8 | 2.9 | 74.4 | 17.4 | 82.4 |
| SHASAM(w/ FLCMI, ViT) | 5.3 | 84.0 | 9.9 | 82.3 | 3.0 | 85.6 | 3.7 | 89.2 | 2.8 | 88.2 | 1.6 | 86.8 | 2.2 | 74.3 | 14.6 | 82.4 |

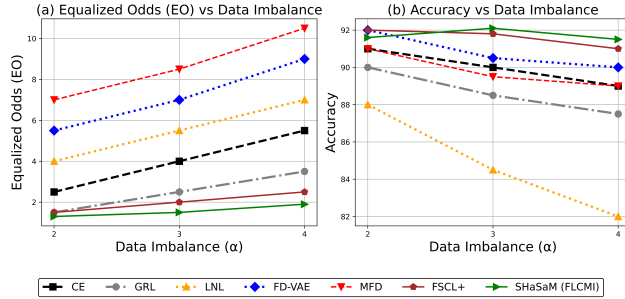


Figure 3. **Results of SHASAM on UTKFace dataset** measuring (a) Equalized Odds and (b) Top-1 Acc. under varying inter-group imbalance (α). The target and sensitive attributes are set to *gender* and *ethnicity* respectively following setup in Park et al. [48].

in Top-1 Accuracy, all of them demonstrate significantly high EO indicating unfair predictions. Compared to SoTA method FSCL, SHASAM (with FLCMI) observes up to 2.7 point reduction in EO with a max. of 2.95% boost in accuracy when the backbone architecture was chosen as ResNet-18 [18]. Replacing the ResNet-18 based encoder with a ViT [11] encoder we continue to observe up to 1.9 points reduction in EO with a 4.1% boost in performance. Further contrasting against FairViT which proposes a novel backbone architecture insensitive to sensitive attributes, SHASAM achieves up to 2.8 points reduction in EO without compromising accuracy gains. Our FL based learning strategy indicated as SHASAM w/ FLCMI shows the highest improvement in fairness with competitive boosts in Top-1 accuracy over SoTA methods.

Further, we compare the resilience of SHASAM in overcoming imbalance between sensitive attribute groups. To this end we vary the imbalance ratio α between sensitive attribute groups in the UTKFace dataset among 2,3,4 and report the top-1 accuracy and EO through Fig. 3(b) and Fig. 3(a). We show that our SHASAM w/ FLCMI approach shows improvements in both EO and accuracy under varying degrees of imbalance. This clearly demonstrates the effectiveness of SHASAM in learning fair representations

Table 3. **Ablation on components in SHASAM** measured in terms of Top-1 Accuracy (Acc.) and equalized odds (EO) by varying the target T and sensitive attributes S on CelebA dataset. Here, FL indicates FLCMI and LD indicates LogDetCMI functions.

| Selection Strategy | Learning Objective | $T = a / S = m$ | | $T = a / S = y$ | |
|--------------------|--------------------|-----------------|-------------|-----------------|-------------|
| | | EO (↓) | Acc. (↑) | EO (↓) | Acc. (↑) |
| Random | SupCon [31] | 30.5 | 80.5 | 21.7 | 80.1 |
| Random | FSCL [48] | 6.5 | 79.1 | 12.4 | 79.1 |
| Random | SHASAM-LEARN (LD) | 6.2 | 79.4 | 11.2 | 79.1 |
| Random | SHASAM-LEARN (FL) | 5.7 | 80.3 | 9.0 | 79.4 |
| SHASAM-MINE (FL) | SupCon [31] | 24.6 | 81.5 | 14.3 | 81.0 |
| SHASAM-MINE (FL) | FSCL [48] | 5.9 | 79.0 | 9.9 | 79.3 |
| SHASAM-MINE (LD) | SHASAM-LEARN (FL) | 6.1 | 78.8 | 10.6 | 77.8 |
| SHASAM-MINE (LD) | SHASAM-LEARN (LD) | 6.1 | 80.7 | 9.9 | 78.6 |
| SHASAM-MINE (FL) | SHASAM-LEARN (FL) | 5.6 | 81.3 | 9.88 | 79.58 |

from the target classes without biasing on the features from sensitive classes.

4.2. Ablation Study

Components in SHASAM In this section we contrast the two main components of SHASAM - SHASAM-MINE and SHASAM-LEARN against baseline method FSCL to demonstrate the effectiveness of our hard sample modeling formulation. At first, we consider random sampling of anchors, positives and negatives, a common practice in the field [31, 48, 58] while varying the learning strategy. We observe in Tab. 3 that SHASAM-LEARN provides significant gains (reduction here) in EO over baselines while demonstrating marginal gains in accuracy. Next, we keep the learning strategy constant (SHASAM-LEARN) and vary the hard sample mining between random and SHASAM-MINE. Enforcing a large decision boundary between target groups while learning features invariant to sensitive attributes through the joint selection and learning formulation in SHASAM demonstrates the best accuracy and EO over baselines.

Sample Selection in SHASAM-MINE We qualify the effectiveness of SHASAM-MINE by conducting experiments on a 2-cluster (denoted as A and B respectively) imbalanced (imbalance ratio $\alpha=5$) synthetic dataset represent-

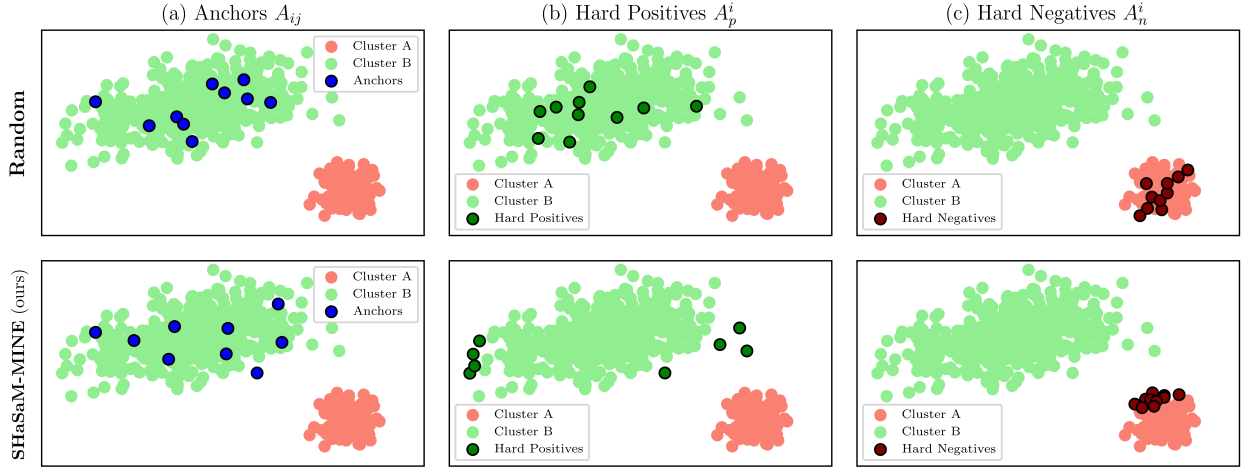


Figure 4. **Contrasting Random and SHASAM-MINE selection strategies** on a synthetic two-cluster imbalanced dataset to identify (a) Anchors, (b) Hard Positives and (c) Hard Negatives, showing the effectiveness of SHASAM in modeling the decision boundary between target attributes. The dataset generation and sample selection is performed under the same seed.

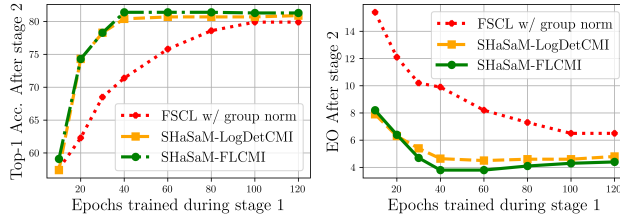


Figure 5. The set formulation in SHASAM learns discriminative representations **within fewer training epochs** (in stage 1) in CelebA for *male* and *attractiveness* as target and sensitive attributes.

ing target attributes. We contrast SHASAM-MINE against random selection which is a common practice in most recent works [48, 58, 63]. Fig. 4 depicts the selected anchors, positives and negatives by both *Random* and SHASAM-MINE strategies with the target class selected as A . Our SHASAM-MINE selects diverse anchors from the target attribute class while selecting hard positives (samples located farthest to the anchor within the target cluster) and hard negatives (samples located closest to the anchors outside the target cluster) which random sampling fails to guarantee. Minimizing L_{SHASAM} with hard positives and negatives (which lie on the cluster boundary) mined through SHASAM-MINE ensures sufficient inter-attribute separation, a critical feature in fair representation learning. We provide more details in the Appendix.

Convergence of SHASAM-LEARN Through Fig. 5 we compare the number of training epochs in stage 1 required to learn discriminative feature representations for various instances of SHASAM against baseline FSCL (with group-normalization). Keeping the experimental settings same as Sec. 4 and batch size at 96 across methods we train F for

specific number of epochs in the range of [10, 100] in stage 1 while training Clf in stage 2 for 10 epochs. The reported accuracy and EO values are reported on the CelebA dataset with *gender* (male or not) and *attractiveness* as target and sensitive attribute respectively. We show that **SHASAM (with FLCMI based learning objective) achieves similar performance to FSCL within fewer epochs** in stage 1. Nevertheless, the joint selection and learning strategy in SHASAM potentially increases per iteration wall-clock time, further discussed in the Appendix.

5. Conclusion

In conclusion, we introduce **SHASAM**, a novel combinatorial framework that addresses the critical challenge of fairness in facial attribute recognition by framing fairness-driven representation learning as a submodular hard-sample mining problem. Through its two-stage approach—SHASAM-MINE and SHASAM-LEARN—our framework leverages submodular functions to select balanced sets of hard-positive and hard-negative samples, mitigating attribute imbalance and preventing sensitive attributes from influencing the learned representations. By minimizing the Conditional Mutual Information between target and sensitive attributes, SHASAM-LEARN enhances fairness while preserving downstream performance. Empirical results on popular benchmarks demonstrate that SHASAM improves fairness (with up to 2.7 point improvement in Equalized Odds) within fewer training epochs compared to existing methods. This work highlights the potential of combinatorial viewpoint in advancing fairness in facial attribute recognition.

Acknowledgements

We gratefully thank anonymous reviewers for their valuable comments. We would also like to extend our gratitude to our fellow researchers from the CARAML lab at UT Dallas for their suggestions. This work is supported by the National Science Foundation under Grant Numbers IIS-2106937, a gift from Google Research, an Amazon Research Award, and the Adobe Data Science Research award. Any opinions, findings, and conclusions or recommendations expressed in this material are those of the authors and do not necessarily reflect the views of the National Science Foundation, Google or Adobe.

References

- [1] Martin Arjovsky, Léon Bottou, Ishaaan Gulrajani, and David Lopez-Paz. Invariant risk minimization. *ArXiv*, abs/1907.02893, 2019. [2](#)
- [2] Eric Baum and Frank Wilczek. Supervised learning of probability distributions by neural networks. In *Neural Information Processing Systems*, 1987. [6](#), [7](#), [12](#), [21](#)
- [3] Nathan Beck, Durga Sivasubramanian, Apurva Dani, Ganesh Ramakrishnan, and Rishabh K. Iyer. Effective evaluation of deep active learning on image classification tasks. *ArXiv*, abs/2106.15324, 2021. [3](#)
- [4] Jeff Bilmes. Submodularity in machine learning and artificial intelligence. *ArXiv*, abs/2202.00132, 2022. [3](#), [4](#)
- [5] Ting Chen, Simon Kornblith, Mohammad Norouzi, and Geoffrey Hinton. A simple framework for contrastive learning of visual representations. *Intl. Conf. on Machine Learning (ICML)*, 2020. [1](#), [3](#), [12](#)
- [6] Xinlei Chen, Haoqi Fan, Ross Girshick, and Kaiming He. Improved baselines with momentum contrastive learning. *arXiv preprint arXiv:2003.04297*, 2020. [3](#), [12](#)
- [7] Elliot Creager, David Madras, Joern-Henrik Jacobsen, Marissa Weis, Kevin Swersky, Toniann Pitassi, and Richard Zemel. Flexibly fair representation learning by disentanglement. In *Proceedings of the 36th International Conference on Machine Learning*, pages 1436–1445, 2019. [2](#), [3](#)
- [8] Jiequan Cui, Zhisheng Zhong, Zhuotao Tian, Shu Liu, Bei Yu, and Jiaya Jia. Generalized parametric contrastive learning. *IEEE Transactions on Pattern Analysis and Machine Intelligence*, pages 1–12, 2023. [2](#)
- [9] Jiankang Deng, Jia Guo, Niannan Xue, and Stefanos Zafeiriou. Arcface: Additive angular margin loss for deep face recognition. In *Proceedings of the IEEE/CVF Conference on Computer Vision and Pattern Recognition*, pages 4690–4699, 2019. [12](#)
- [10] Alexey Dosovitskiy, Lucas Beyer, Alexander Kolesnikov, Dirk Weissenborn, Xiaohua Zhai, Thomas Unterthiner, Mostafa Dehghani, Matthias Minderer, Georg Heigold, Sylvain Gelly, Jakob Uszkoreit, and Neil Houlsby. An image is worth 16x16 words: Transformers for image recognition at scale. In *International Conference on Learning Representations*, 2021. [1](#), [6](#), [7](#), [14](#)
- [11] Alexey Dosovitskiy, Lucas Beyer, Alexander Kolesnikov, Dirk Weissenborn, Xiaohua Zhai, Thomas Unterthiner, Mostafa Dehghani, Matthias Minderer, Georg Heigold, Sylvain Gelly, Jakob Uszkoreit, and Neil Houlsby. An image is worth 16x16 words: Transformers for image recognition at scale. In *International Conference on Learning Representations*, 2021. [1](#), [6](#), [7](#), [14](#)
- [12] Fei Du, Peng Yang, Qi Jia, Fengtao Nan, Xiaoting Chen, and Yun Yang. Global and local mixture consistency cumulative learning for long-tailed visual recognitions. In *Proceedings of the IEEE/CVF Conference on Computer Vision and Pattern Recognition (CVPR)*, pages 15814–15823, 2023. [2](#)
- [13] Sivasubramanian Durga, Rishabh Iyer, Ganesh Ramakrishnan, and Abir De. Training data subset selection for regression with controlled generalization error. In *International Conference on Machine Learning*, pages 9202–9212. PMLR, 2021. [3](#)
- [14] Nicholas Frosst, Nicolas Papernot, and Geoffrey E. Hinton. Analyzing and improving representations with the soft nearest neighbor loss. In *International Conference on Machine Learning*, 2019. [12](#)
- [15] Satoru Fujishige. *Submodular Functions and Optimization*. Elsevier, 2005. [2](#), [3](#), [4](#), [12](#)
- [16] Michael Gutmann and Aapo Hyvärinen. Noise-contrastive estimation: A new estimation principle for unnormalized statistical models. In *Proceedings of the Thirteenth International Conference on Artificial Intelligence and Statistics*, pages 297–304. PMLR, 2010. [12](#)
- [17] Moritz Hardt, Eric Price, and Nathan Srebro. Equality of opportunity in supervised learning. In *Proceedings of the 30th International Conference on Neural Information Processing Systems*, page 3323–3331, 2016. [6](#)
- [18] Kaiming He, Xiangyu Zhang, Shaoqing Ren, and Jian Sun. Deep Residual Learning for Image Recognition. In *IEEE Conf. on Computer Vision and Pattern Recognition (CVPR)*, 2016. [1](#), [6](#), [7](#)
- [19] Kaiming He, Haoqi Fan, Yuxin Wu, Saining Xie, and Ross Girshick. Momentum contrast for unsupervised visual representation learning. In *2020 IEEE/CVF Conference on Computer Vision and Pattern Recognition (CVPR)*, 2020. [1](#), [3](#), [12](#)
- [20] Rishabh Iyer and Jeff Bilmes. Polyhedral aspects of submodularity, convexity and concavity. *ArXiv*, abs/1506.07329. [3](#)
- [21] Rishabh Iyer, Ninad Khargonkar, Jeff Bilmes, and Himanshu Asanani. Submodular combinatorial information measures with applications in machine learning. In *Algorithmic Learning Theory*, pages 722–754. PMLR, 2021. [4](#)
- [22] Rishabh Iyer, Ninad Khargonkar, Jeff Bilmes, and Himanshu Asanani. Generalized submodular information measures: Theoretical properties, examples, optimization algorithms, and applications. *IEEE Transactions on Information Theory*, 68(2):752–781, 2021. [4](#)
- [23] Eeshaan Jain, Tushar Nandy, Gaurav Aggarwal, Ashish V. Tendulkar, Rishabh K Iyer, and Abir De. Efficient data subset selection to generalize training across models: Transductive and inductive networks. In *Thirty-seventh Conference on Neural Information Processing Systems (NeurIPS)*, 2023. [3](#), [12](#)

[24] Stefanie Jegelka and Jeff Bilmes. Submodularity beyond submodular energies: Coupling edges in graph cuts. In *CVPR*, 2011. 2, 12

[25] Sangwon Jung, Donggyu Lee, Taeeon Park, and Taesup Moon. Fair feature distillation for visual recognition. In *2021 IEEE/CVF Conference on Computer Vision and Pattern Recognition (CVPR)*, 2021. 3, 6, 7, 14, 21

[26] Athresh Karanam, Krishnateja Killamsetty, Harsha Kokel, and Rishabh Iyer. ORIENT: Submodular mutual information measures for data subset selection under distribution shift. In *Advances in Neural Information Processing Systems (NeurIPS)*, 2022. 5

[27] V. Kaushal, R. Iyer, K. Doctor, A. Sahoo, P. Dubal, S. Kothawade, R. Mahadev, K. Dargan, and G. Ramakrishnan. Demystifying multi-faceted video summarization: Tradeoff between diversity, representation, coverage and importance. In *2019 IEEE Winter Conference on Applications of Computer Vision (WACV)*, pages 452–461, 2019. 2, 4, 5, 12

[28] Vishal Kaushal, Rishabh Iyer, Suraj Kothawade, Rohan Mahadev, Khoshrav Doctor, and Ganesh Ramakrishnan. Learning from less data: A unified data subset selection and active learning framework for computer vision. In *2019 IEEE Winter Conference on Applications of Computer Vision (WACV)*, 2019. 3

[29] Vishal Kaushal, Sandeep Subramanian, Suraj Kothawade, Rishabh Iyer, and Ganesh Ramakrishnan. A framework towards domain specific video summarization. In *2019 IEEE winter conference on applications of computer vision (WACV)*, pages 666–675. IEEE, 2019. 4, 12

[30] Vishal Kaushal, Suraj Kothawade, Anshul Tomar, Rishabh Iyer, and Ganesh Ramakrishnan. How good is a video summary? a new benchmarking dataset and evaluation framework towards realistic video summarization. *ArXiv*, abs/2101.10514, 2021. 4

[31] Prannay Khosla, Piotr Teterwak, Chen Wang, Aaron Sarna, Yonglong Tian, Phillip Isola, Aaron Maschinot, Ce Liu, and Dilip Krishnan. Supervised contrastive learning. In *Advances in Neural Information Processing Systems*, 2020. 1, 3, 6, 7, 12, 14, 21

[32] Krishnateja Killamsetty, Changbin Li, Chen Zhao, Feng Chen, and Rishabh Iyer. A nested bi-level optimization framework for robust few shot learning. In *Proceedings of the AAAI Conference on Artificial Intelligence*, pages 7176–7184, 2022. 3

[33] Krishnateja Killamsetty, Guttu Sai Abhishek, Aakriti, Ganesh Ramakrishnan, Alexandre V. Evfimievski, Lucian Popa, and Rishabh Iyer. AUTOMATA: gradient based data subset selection for compute-efficient hyper-parameter tuning. In *Proceedings of the 36th International Conference on Neural Information Processing Systems*, 2024. 3, 12

[34] Byungu Kim, Hyunwoo Kim, Kyungsu Kim, Sungjin Kim, and Junmo Kim. Learning not to learn: Training deep neural networks with biased data. In *The IEEE Conference on Computer Vision and Pattern Recognition (CVPR)*, 2019. 2, 6, 7, 14, 21

[35] Suraj Kothawade, Saikat Ghosh, Sumit Shekhar, Yu Xiang, and Rishabh K. Iyer. Talisman: Targeted active learning for object detection with rare classes and slices using submodular mutual information. In *Computer Vision - ECCV 2022 - 17th European Conference*, 2022. 2, 3

[36] Suraj Kothawade, Vishal Kaushal, Ganesh Ramakrishnan, Jeff A. Bilmes, and Rishabh K. Iyer. PRISM: A rich class of parameterized submodular information measures for guided data subset selection. In *Thirty-Sixth AAAI Conference on Artificial Intelligence, AAAI*, pages 10238–10246, 2022. 2, 3, 5, 12

[37] Matt J Kusner, Joshua Loftus, Chris Russell, and Ricardo Silva. Counterfactual fairness. In *Advances in Neural Information Processing Systems (NeurIPS)*, 2017. 6

[38] Kimmo Kärkkäinen and Jungseock Joo. FairFace: Face attribute dataset for balanced race, gender, and age for bias measurement and mitigation. In *Proceedings of the IEEE/CVF Winter Conference on Applications of Computer Vision*, pages 1548–1558, 2021. 1, 2

[39] Hui Lin and Jeff Bilmes. A class of submodular functions for document summarization. In *Proceedings of the 49th Annual Meeting of the Association for Computational Linguistics: Human Language Technologies*, 2011. 2, 12

[40] Ziwei Liu, Ping Luo, Xiaogang Wang, and Xiaoou Tang. Deep learning face attributes in the wild. In *Proceedings of International Conference on Computer Vision (ICCV)*, 2015. 1, 6

[41] David Madras, Elliot Creager, Toniann Pitassi, and Richard Zemel. Learning adversarially fair and transferable representations. In *Proceedings of the 35th International Conference on Machine Learning*, pages 3384–3393. PMLR, 2018. 3

[42] Anay Majee, Suraj Nandkishor Kothawade, Krishnateja Killamsetty, and Rishabh K Iyer. SCoRe: Submodular combinatorial representation learning. In *Proceedings of the 41st International Conference on Machine Learning*, pages 34327–34349, 2024. 2, 3, 4, 5, 6, 13, 18

[43] Anay Majee, Ryan Sharp, and Rishabh Iyer. SMILE: Leveraging submodular mutual information for robust few-shot object detection. In *European Conference on Computer Vision (ECCV)*, 2024. 2, 3, 4, 5, 13

[44] Baharan Mirzasoleiman, Ashwinkumar Badanidiyuru, Amin Karbasi, Jan Vondrak, and Andreas Krause. Lazier than lazy greedy. *Proceedings of the AAAI Conference on Artificial Intelligence*, 29(1), 2015. 4, 5, 13

[45] G. L. Nemhauser, L. A. Wolsey, and M. L. Fisher. An analysis of approximations for maximizing submodular set functions—i. *Mathematical Programming*, 14(1):265–294, 1978. 4, 13, 18

[46] Patrik Orlanovic, Roger Waleffe, Vasilis Mageirakos, Konstantinos Nikolakakis, Amin Karbasi, Dionysios Kalogerias, Nezihe Merve Gürel, and Theodoros Rekatsinas. Repeated random sampling for minimizing the time-to-accuracy of learning. In *The Twelfth International Conference on Learning Representations*, 2024. 14

[47] Sungho Park, Sunhee Hwang, Dohyung Kim, and Hyeran Byun. Learning disentangled representation for fair facial attribute classification via fairness-aware information alignment. *Proceedings of the AAAI Conference on Artificial Intelligence*, 35(3):2403–2411, 2021. 3, 6, 7, 14, 21

[48] Sungho Park, J ewook Lee, Pilhyeon Lee, Sunhee Hwang, Dohyung Kim, and Hyeran Byun. Fair contrastive learning for facial attribute classification. In *2022 IEEE/CVF Conference on Computer Vision and Pattern Recognition (CVPR)*, 2022. 1, 2, 3, 6, 7, 8, 14, 17, 18, 19, 21

[49] Momchil Peychev, Anian Ruoss, Mislav Balunović, Maximilian Baader, and Martin Vechev. Latent space smoothing for individually fair representations. In *Computer Vision – ECCV 2022*, page 535–554, 2022. 3

[50] Yao Qiang, Chengyin Li, Prashant Khanduri, and Dongxiao Zhu. Fairness-aware vision transformer via debiased self-attention. In *Computer Vision – ECCV 2024*, page 358–376, 2024. 3

[51] Edward Raff and Jared Sylvester. Gradient reversal against discrimination: A fair neural network learning approach. In *2018 IEEE 5th International Conference on Data Science and Advanced Analytics (DSAA)*, page 189–198. IEEE, 2018. 2, 6, 7, 14, 21

[52] Vikram V. Ramaswamy, Sunnie S. Y. Kim, and Olga Russakovsky. Fair attribute classification through latent space de-biasing. In *Proceedings of the IEEE/CVF Conference on Computer Vision and Pattern Recognition (CVPR)*, pages 9301–9310, 2021. 3, 18

[53] Kanchana Ranasinghe, Muzammal Naseer, Munawar Hayat, Salman Khan, and Fahad Shahbaz Khan. Orthogonal projection loss. In *Proceedings of the IEEE/CVF International Conference on Computer Vision (ICCV)*, 2021. 12

[54] Yuji Roh, Weili Nie, De-An Huang, Steven Euijong Whang, Arash Vahdat, and Anima Anandkumar. Dr-fairness: Dynamic data ratio adjustment for fair training on real and generated data. *Transactions on Machine Learning Research*, 2023. 3

[55] Yaniv Romano, Stephen Bates, and Emmanuel J. Candès. Achieving equalized odds by resampling sensitive attributes. In *Advances in Neural Information Processing Systems*, pages 361–371, 2020. 2

[56] Mhd Hasan Sarhan, Nassir Navab, Abouzar Eslami, and Shadi Albarqouni. Fairness by learning orthogonal disentangled representations. In *Computer Vision – ECCV 2020*, page 746–761, 2020. 2

[57] Florian Schroff, Dmitry Kalenichenko, and James Philbin. FaceNet: A unified embedding for face recognition and clustering. In *IEEE Conf. on Computer Vision and Pattern Recognition (CVPR)*, 2015. 12

[58] Aili Shen, Xudong Han, Trevor Cohn, Timothy Baldwin, and Lea Frermann. Contrastive learning for fair representations. *ArXiv*, abs/2109.10645, 2021. 1, 3, 6, 7, 8, 14

[59] Yujun Shen, Ceyuan Yang, Xiaou Tang, and Bolei Zhou. InterFaceGAN: Interpreting the disentangled face representation learned by gans. *TPAMI*, 2020. 2

[60] Kihyuk Sohn. Improved deep metric learning with multi-class n-pair loss objective. In *Advances in Neural Inf. Processing Systems*, 2016. 12

[61] Hyun Oh Song, Yu Xiang, Stefanie Jegelka, and Silvio Savarese. Deep metric learning via lifted structured feature embedding. In *Computer Vision and Pattern Recognition (CVPR)*, 2016. 4, 12

[62] Sruthi Sudhakar, Viraj Prabhu, Arvindkumar Krishnakumar, and Judy Hoffman. Mitigating bias in visual transformers via targeted alignment. *ArXiv*, abs/2302.04358, 2023. 3, 7

[63] Bowei Tian, Ruijie Du, and Yanning Shen. Fairvit: Fair vision transformer via adaptive masking, 2024. 2, 3, 6, 7, 8, 14, 18, 19, 21

[64] Christina Wadsworth, Francesca Vera, and Chris Piech. Achieving fairness through adversarial learning: an application to recidivism prediction. *ArXiv*, abs/1807.00199, 2018. 2

[65] Hao Wang, Yitong Wang, Zheng Zhou, Xing Ji, Dihong Gong, Jingchao Zhou, Zhifeng Li, and Wei Liu. Cosface: Large margin cosine loss for deep face recognition. In *Proceedings of the IEEE Conference on Computer Vision and Pattern Recognition (CVPR)*, 2018. 12

[66] Xun Wang, Xintong Han, Weilin Huang, Dengke Dong, and Matthew R Scott. Multi-similarity loss with general pair weighting for deep metric learning. In *Proc. of the IEEE Conf. on Computer Vision and Pattern Recognition*, 2019. 12

[67] Zeyu Wang, Klint Qinami, Ioannis Christos Karakozis, Kyle Genova, Prem Nair, Kenji Hata, and Olga Russakovsky. Towards fairness in visual recognition: Effective strategies for bias mitigation. In *2020 IEEE/CVF Conference on Computer Vision and Pattern Recognition (CVPR)*, 2020. 2

[68] Kai Wei, Rishabh Iyer, and Jeff Bilmes. Submodularity in data subset selection and active learning. In *ICML*, 2015. 3

[69] Zhifei Zhang, Yang Song, and Hairong Qi. Age progression/regression by conditional adversarial autoencoder. In *IEEE Conference on Computer Vision and Pattern Recognition (CVPR)*, 2017. 1, 6

[70] Jieyu Zhao, Tianlu Wang, Mark Yatskar, Vicente Ordonez, and Kai-Wei Chang. Men also like shopping: Reducing gender bias amplification using corpus-level constraints. In *Proceedings of the 2017 Conference on Empirical Methods in Natural Language Processing*, pages 2979–2989, 2017. 2

Appendices

| | |
|---|-----------|
| A Notation | 12 |
| B Additional Related Work and Preliminaries | 12 |
| B.1. Contrastive Learning | 12 |
| B.2. Submodularity (Cont. from Section 3.2) . . . | 12 |
| C Additional Explanation to Fig. 1 | 13 |
| D Additional Implementation Details | 13 |
| D.1. Settings for Selection in SHASAM-MINE . . | 14 |
| D.2. Training and Evaluation in SHASAM-LEARN | 14 |
| D.3. Experiments on Synthetic Dataset | 14 |
| E Gradients through $L_{\text{SHASAM}}(\theta)$ | 14 |

| | |
|---|-----------|
| F. Derivation of Instances of SHASAM | 15 |
| F.1. SHASAM-FLCMI | 15 |
| F.2. SHASAM-LogDetCMI | 16 |
| G Additional Fairness Metrics (Contd. from Sec. 4) | 17 |
| H Additional Results | 17 |
| H.1. Additional Results from Metrics in Appendix G | 17 |
| H.2. Comparison against FairViT on UTKFace Dataset | 18 |
| H.3. Ablation on the selection Budget | 18 |
| H.4. Ablation: Choice of Combinatorial Function in SHASAM | 18 |
| H.5. Ablation: Compute Cost and Wall Clock time | 19 |
| H.6. Characterization of SHASAM-MINE on Synthetic Data | 19 |
| H.7. Standard Deviation of Results on CelebA | 19 |

I. Limitations

A. Notation

Following the problem definition in the main paper we introduce the notations used in Tab. 4 throughout the paper.

B. Additional Related Work and Preliminaries

B.1. Contrastive Learning

In the realm of supervised learning, conventional models utilizing Cross-Entropy (CE) loss [2] often grapple with challenges posed by class imbalance and noisy labels. To address these issues, metric learning techniques [9, 53, 65, 66] aim to learn distance-based [57] or similarity-based [9, 65] metrics, fostering orthogonality within the feature space [53] and bolstering class-specific feature discrimination. Contrastive learning, rooted in noise contrastive estimation [16], has become a cornerstone in self-supervised learning [5, 6, 19], where label information is unavailable during training. In supervised contexts, SupCon [31] emphasizes forming feature clusters rather than merely aligning features to predefined centroids. For instance, Triplet loss [57] differentiates one positive and one negative pair, whereas N-pairs [60] loss incorporates multiple negative pairs, and SupCon extends this by leveraging multiple positive and negative pairs. Lifted-Structure loss [61] sharpens focus by contrasting positives against the hardest negatives, and SupCon exhibits similarities with Soft-Nearest Neighbors loss [14], which maximizes inter-class entanglements. Despite the significant achievements of these methods, they predominantly rely on pairwise similarity metrics, which may not inherently facilitate the formation of disjoint clusters.

B.2. Submodularity (Cont. from Section 3.2)

As discussed in Sec. 3.2 of the main paper, submodular functions have been recognized to model notions of cooperation [24], diversity [39], representation [36] and coverage [27]. Following the combinatorial formulation in Sec.3.1 of the main paper we define the ground set $\mathcal{V} = \{T_1, T_2, \dots, T_N\} = \{S_1, S_2, \dots, S_K\}$ and explore four different categories of submodular information functions in our work, namely -

(1) *Submodular Total Information* (S_f) which measures the total information contained in each set [15], expressed as $S_f(T_1, T_2, \dots, T_N)$ as in Eq. (4). Maximizing S_f over a set T_i models diversity [39] while minimizing S_f models cooperation [24].

$$S_f(T_1, T_2, \dots, T_N) = \sum_{i=1}^N f(T_i) \quad (4)$$

(2) *Submodular Mutual Information* (I_f) which models the shared information between two sets [36] which serves as a measure of *similarity/cooperation* between them, expressed through Eq. (5).

$$I_f(T_i; T_j) = f(T_i) + f(T_j) - f(T_i \cup T_j), \forall i, j \in |\mathcal{V}| \quad (5)$$

(3) *Submodular Conditional Gain* (H_f) which models the gain in information when a set T_j is added to T_i . H_f models the notion of *dissimilarity* between sets and can be expressed in Eq. (6).

$$\begin{aligned} H_f(T_i|T_j) &= f(T_i \cup T_j) - f(T_j) \\ &= f(T_i) - I_f(T_i; T_j), \forall i, j \in |\mathcal{V}| \end{aligned} \quad (6)$$

(4) *Submodular Conditional Mutual Information* (I_f) which jointly models the mutual similarity between two sets T_i and T_j and their collective dissimilarity to a conditioning set C as:

$$\begin{aligned} I_f(T_i; T_j|C) &= f(T_i \cup C) + f(T_j \cup C) \\ &\quad - f(T_i \cup T_j \cup C) - f(C) \\ I_f(T_i; T_j|C) &= I_f(T_i \cup C; T_j) - I_f(T_j; C) \\ &= H_f(T_i|C) + H_f(T_j|C) \\ &\quad - H_f(T_i \cup T_j|C), \forall i, j \in |\mathcal{V}| \end{aligned} \quad (7)$$

Note, that the above formulations can also be reformulated by considering the sensitive attribute S_i instead of T_i , $\mathcal{V} = \cup_{i=1}^N T_i = \cup_{j=1}^K S_j$. Given a submodular function f (can alternatively be I_f or H_f) tasks like selection [23, 33] and summarization [27, 29] have been modeled as a discrete optimization problem to identify a summarized set of examples $A \subseteq \mathcal{V}$ via submodular maximization under a cardinality constraint ($|A| \leq k$), i.e.

Table 4. Collection of notations used in the paper.

| Symbol | Description |
|----------------------|---|
| \mathcal{V} | The Ground set, here refers to the mini-batch at each iteration. |
| T_i | The target attribute set $T_i, \forall i \in \mathcal{V} $. |
| S_j | The sensitive attribute set $S_j, \forall j \in \mathcal{V} $. |
| A_{ij} | Anchor set with examples from target attribute T_i and sensitive attribute S_j . |
| A_p^i | Hard-Positives with examples from target attribute T_i and sensitive attribute $\overline{S_j}$. |
| A_n^i | Hard-Negatives with examples from target attribute $\mathcal{V} \setminus T_i$ and sensitive attribute S_j . |
| $F(x, \theta)$ | Neural Network used as feature extractor. |
| $Clf(\cdot, \cdot)$ | Multi-Layer Perceptron as classifier. In our case a two layer network. |
| θ | Parameters of the feature extractor. |
| $S_{A,B}(\theta)$ | Cross-Similarity between sets $A, B \in \mathcal{V}$. |
| $S_A(\theta)$ | Self-Similarity between samples in set $A \in \mathcal{T}$. |
| $f(A)$ | Submodular Information function over a set A . |
| $I_f(A; Q)$ | Submodular Mutual Information function between sets A and Q . |
| $H_f(A Q)$ | Submodular Conditional Gain function between sets A and Q . |
| $I_f(A; Q P)$ | Submodular Conditional Mutual Information function between a target set A , query set Q and private set P . |
| $L_{SHASAM}(\theta)$ | Loss value computed over all target and sensitive attribute pairs. |
| $N_f(A_{ij})$ | Normalization constant approximated to $3 A_{ij} $. |
| EO | Equalized Odds. |

$\max_{A \subseteq \mathcal{V}, |A| \leq k} f(A)$. This can be fairly approximated with a $(1 - e^{-1})$ constant factor guarantee [45] using greedy optimization techniques [44] as shown in Appendix B.2. Extending the definition of submodular functions to continuous optimization space Majee et al. [42] have proposed a set of novel family of learning objectives which minimize total information and total correlation among sets in D_{train} using continuous optimization techniques like SGD. These objectives have been shown to be significantly more robust to large imbalance demonstrated in real-world tasks like longtail recognition [42] and few-shot learning [43].

Algorithm 2 Greedy Submodular Maximization as in Nemhauser et al. [45].

Require: Submodular function $f : 2^{\mathcal{V}} \rightarrow \mathbb{R}$, cardinality constraint k
Ensure: Set $A \subseteq \mathcal{V}$ maximizing $f(A)$ under cardinality constraint k

- 1: Initialize an empty set $A \leftarrow \emptyset$
- 2: **for** $j = 1$ to k **do**
- 3: $e \leftarrow \underset{v \in \mathcal{V} \setminus A}{\operatorname{argmax}} (f(A \cup \{v\}) - f(A))$
- 4: $A \leftarrow A \cup \{e\}$
- 5: **end for**
- 6: **return** A

C. Additional Explanation to Fig. 1

In this section we elaborate the steps of operation of SHASAM which is condensed and depicted in Fig. 1 of the main paper. At first, given a ground set (a large labeled pool) \mathcal{V} we would like to mine an anchor set A_{12} .

Anchor sets are supposed to contain examples sharing the same target and sensitive attributes T_1 and S_2 as shown in Fig. 1. In our example T_1 refers to males and $\overline{T_1}$ refers to non-males. Similarly S_2 refers to males wearing sunglasses and $\overline{S_2}$ refers to people (irrespective of gender) that do not wear sunglasses. Thus, A_{12} contains examples of males wearing eyeglasses. Once we have the anchor set, we now use the formulation described in Sec. 3.3 we mine A_p^1 which resembles the hard-positives containing examples of males which do not wear eyeglasses. Similarly we now mine hard-negatives A_n^1 which contain examples of females (or $\overline{T_1}$) who wear eyeglasses as shown in Fig. 1(a). This is the operation of SHASAM-MINE.

Once we have mined A_{12} , A_p^1 and A_n^1 we now would like to learn embedding separation between A_{12} and A_n^1 while bringing A_p^1 closer to A_{12} . As shown in Fig. 1(b) we apply SHASAM-LEARN which is a loss function derived from Submodular Conditional Mutual Information (SCMI) as shown in eq. 3 of the main paper. Following the discussion in Sec. 3.5 SCMI based learning objectives jointly model anchor-hard-negative separation while modeling anchor-hard-positive cooperation when minimized used SGD. With sufficient training SHASAM-LEARN results in an embedding space which learns the decision boundary between males and non-males without biasing on the sensitive attribute - wearing sunglasses as shown in Fig. 1(b).

D. Additional Implementation Details

The implementation details are largely elucidated in Sec. 4 of the main paper but we add more details below and at https://anaymajee.me/assets/project_pages/shasam.html.

D.1. Settings for Selection in SHASAM-MINE

As discussed in Algorithm 1 of the main paper we employ three different submodular functions to sample the anchors A_{ij} , hard-positives A_p^i and hard-negatives A_n^i . We run the selection at every iteration of the training process with 16 anchors, 16 hard-positives and 16 hard-negatives selected in each iteration. Each image further gets augmented into two views which results in a batch size of 96 as discussed in Sec. 4 of the main paper. Following our problem formulation, at each iteration we randomly select a target attribute T_i and a sensitive attribute S_j where $i, j \in |\mathcal{V}|$. All anchors in A_{ij} share the same target and sensitive attribute, thus mined from $T_i \cap S_j$, while the hard-positives share the same target attribute but different sensitive attribute labels from $T_i \cap \overline{S_j}$. Finally, negatives are mined from $\overline{T_i} \cap S_j$ and share orthogonal target attributes while retaining the same sensitive attribute. This formulation follows Park et al. [48] and results in selection of samples at the cluster boundary.

Since the ground set resembles the complete dataset at each iteration, selection of A_{ij} , A_p^i and A_n^i becomes computationally inefficient (large computational cost). To mitigate this situation, we randomly select a subset of the dataset at each epoch and use it for model training. This strategy draws inspiration from Okanovic et al. [46] and significantly improves training speeds without compromising on performance.

D.2. Training and Evaluation in SHASAM-LEARN

As discussed in Sec. 3 of the main paper, SHASAM-MINE and SHASAM-LEARN are sequentially invoked at each iteration for training the feature extractor F on dataset D^{train} . Following the experimental setup in Sec. 4 of the main paper, each image in both CelebA and UTKFace datasets are resized to 128×128 pixels with two complementary augmentations among - RandomCrop, Grayscale, ColorJitters etc. similar to Khosla et al. [31]. For the implementations of GRL [51], LNL [34], FD-VAE [47], MFD [25], FSCL [48] we follow the implementation in Park et al. [48] and report the average Top-1 Accuracy (Acc.) and Equalized Odds (EO) over three random seeds. Particularly in case of FSCL, we adopt their two-stage training strategy to train a ResNet-18 based feature extractor on the train split for 100 epochs with a 0.1 initial learning rate and a cosine annealing scheduler. On the contrary, our SHASAM approach is trained with a higher initial learning rate of 0.4 with a cosine annealing scheduler for ~ 20 epochs during stage 1. For stage 2 both FSCL and SHASAM are trained for 10 epochs, keeping the feature extractor frozen.

For FairViT [63] we adopt a ViT [11] based feature extractor with fairness driven modifications as suggested in the original paper. We perform a single stage training till convergence. Unlike using the first 80 individuals from the CelebA dataset as in the original implementation, we use all

individuals available in CelebA for reproduction of the results. For fair comparisons, we replace the feature extractor in SHASAM (ResNet-18) with a vanilla ViT architecture and conduct two sets of experiments, one following FSCL (denoted as FSCL w/ViT in Table 2) and the other adopting the SHASAM (denoted as SHASAM w/ FLCMI, ViT in Table 2) with Facility-Location Conditional Mutual Information (FLCMI) based learning objective.

D.3. Experiments on Synthetic Dataset

To characterize the selection strategy discussed in Sec. 3.4 (SHASAM-MINE) we conduct experiments on synthetic datasets by varying (1) *imbalance* and (2) *Feature Similarity* (cluster overlap). To this end we introduce a 2-dimensional 2-cluster setting as shown in Fig. 4 of the main paper. For varying imbalance we ablate on the imbalance ratio α from 1 in the balanced setting and 5 in the imbalanced setting. Fig. 4 (main paper) depicts the imbalanced setting with $\alpha = 5$. The abundant cluster A consists of 500 examples with high intra-group variance while the rare class has 100 examples with low intra-group variance. The selection budget was set to 10 examples for each anchor, hard-positive and hard-negative sets. To contrast against *Random* sampling (commonly used strategy in [31, 48, 58]) we keep the seed constant for underlying libraries. Between the imbalanced settings Fig. 4 (main paper) and Fig. 9 (supplementary), we highlight the difference in selected samples by altering the target attribute between the majority and minority class. For the balanced setting (1), α is set to 1 with each cluster containing 200 examples. This is depicted in Fig. 8. The variance of the clusters indicated through the spread of points in the feature space is also kept constant between cluster A and B . For varying the (2) feature similarity we reduce the separation between two clusters so that some overlap exists between them by reducing the 2D distance between the cluster centroids. The imbalance is kept constant at $\alpha = 5$ and the majority class is considered as the target class, similar to setting in Fig. 4 of the main paper. This setting is depicted through Fig. 10 and discussed in detail in Appendix H.6.

E. Gradients through $L_{SHASAM}(\theta)$

In this section we provide proof for our proposed formulation in Sec. 3.2, eq. (2) which states that the gradient through $L_{SHASAM}(\theta) \approx \nabla L_{SHASAM}(A_{ij}, A_p^i, A_n^i, \theta)$ which is the gradient over the combinatorial loss alone.

Proof. At first we can consider the definition of $L_{SHASAM}(\theta)$ as a product of three functions $X(\theta)$, $Y(\theta)$ and $Z(\theta)$ as shown below.

$$\begin{aligned}
L_{\text{SHASAM}}(\theta) &= \sum_{\forall i, j \in |\mathcal{V}|} \underbrace{\text{softmax}(H_f(\cdot | A_{ij}), A_p^i, T_i \cap \overline{S_j}))}_{X(\theta)} \\
&\quad \times \underbrace{\text{softmax}(I_f(\cdot; A_{ij}), A_n^i, \mathcal{V} \setminus T_i \cap S_j)}_{Y(\theta)} \\
&\quad \times \underbrace{L_{\text{SHASAM}}(A_{ij}, A_p^i, A_n^i; \theta)}_{Z(\theta)} \\
L_{\text{SHASAM}}(\theta) &= \sum_{\forall i, j \in |\mathcal{V}|} X(\theta) \times Y(\theta) \times Z(\theta)
\end{aligned} \tag{8}$$

Given this simplified form, we calculate the gradients through $L_{\text{SHASAM}}(\theta)$ following the chain rule as -

$$\begin{aligned}
\frac{\partial L_{\text{SHASAM}}(\theta)}{\partial \theta} &= \frac{\partial X(\theta)}{\partial \theta} \times Y(\theta) \times Z(\theta) \\
&\quad + X(\theta) \times \frac{\partial Y(\theta)}{\partial \theta} \times Z(\theta) \\
&\quad + X(\theta) \times Y(\theta) \times \frac{\partial Z(\theta)}{\partial \theta}
\end{aligned} \tag{9}$$

We know that, $X(\theta)$ and $Y(\theta)$ are hard-positive and hard-negative miners and are approximated as the softmax over the selected subset A from Q given a selection function $F(\cdot)$. Lets call this σ -

$$\sigma_i(\theta) = \text{softmax}(F(\cdot; \theta), A, Q) = \frac{\exp(F_i(A; \theta))}{\sum_j \exp(F_j(A; \theta))} \tag{10}$$

Irrespective of the choice of the selection function $F(\cdot)$ the gradient over σ can be written as -

$$\frac{\partial \sigma_i(\theta)}{\partial F_i(A)} = \begin{cases} \sigma_i(\theta)(1 - \sigma_i(\theta)) & \text{if } i = k, \\ -\sigma_i(\theta)\sigma_k(\theta) & \text{if } i \neq k. \end{cases} \tag{11}$$

In the first case, when $i == k$ the softmax function evaluates to 1 and occurs when $\sigma_i(\theta)$ is approximately the argmax. Similarly, for the second case, $i \neq k$ occurs when $\sigma_i(\theta)$ does not approximate the argmax. In this case $\sigma_i(\theta)$ evaluates to 0. Thus, in both cases the gradients through $X(\theta)$ and $Y(\theta)$ approximate to 0. This reduces the gradient calculation for $L_{\text{SHASAM}}(\theta)$ as -

$$\frac{\partial L_{\text{SHASAM}}(\theta)}{\partial \theta} = X(\theta) \times Y(\theta) \times \frac{\partial Z(\theta)}{\partial \theta} \tag{12}$$

Since $Z(\theta)$ represents the loss function $L_{\text{SHASAM}}(A_{ij}, A_p^i, A_n^i, \theta)$ and thus:

$$\nabla_{\theta} L_{\text{SHASAM}}(\theta) \approx \nabla_{\theta} L_{\text{SHASAM}}(A_{ij}, A_p^i, A_n^i, \theta) \tag{13}$$

Where C is a constant, $C = X(\theta)Y(\theta)$. This proves our consideration in the formulation in Sec. 3.2 and allows SHASAM to utilize a mixture of discrete and continuous optimization problems to model learning of fair representations as a submodular hard sample mining. \square

F. Derivation of Instances of SHASAM

We define the loss function in SHASAM as the conditional mutual information between the mined anchors A_{ij} , hard-positives A_p^i and hard-negatives A_n^i as shown in eq. (3) of the main paper. We summarize it here for readability as Eq. (14).

$$L_{\text{SHASAM}}(\theta) = \sum_{\forall i, j \in |\mathcal{V}|} \frac{1}{N_f(A_{ij})} I_f(A_{ij}; A_n^i | A_p^i; \theta) \tag{14}$$

In this section we derive two important instances of L_{SHASAM} based on the choice of the submodular function $f(A, \theta)$ over set A as summarized in Table 1 of the main paper.

F.1. SHASAM-FLCMI

Given a dataset \mathcal{V} and the Facility-Location (FL) submodular function $f(A) = \sum_{i \in \mathcal{V}} \max_{j \in A} S_{ij}$ over a set A , we derive a combinatorial loss L_{SHASAM} on the mined anchors A_{ij} , hard-positives A_p^i and hard-negatives A_n^i based on the Submodular Conditional Mutual Information function $I_f(A_{ij}; A_n^i | A_p^i)$ as shown in Eq. (15).

$$L_{\text{SHASAM}}(\theta) = \sum_{i, j \in |\mathcal{V}|} \frac{1}{3|A_{ij}|} \max \left(\min \left(\max_{a \in A_{ij}} S_{ia}, \max_{n \in A_n^i} S_{in} \right) - \max_{p \in A_p^i} S_{ip}, 0 \right) \tag{15}$$

Proof. From the definition of CMI based on conditional gain as shown in Eq. (7),

$$\begin{aligned}
I_f(A_{ij}; A_n^i | A_p^i) &= H_f(A_{ij} | A_p^i) + H_f(A_{ij} | A_n^i) \\
&\quad - H_f(A_{ij} \cup A_n^i | A_p^i) \\
&= f(A_{ij}) - I_f(A_{ij}; A_p^i) \\
&\quad + f(A_{ij}) - I_f(A_{ij}; A_n^i) \\
&\quad - f(A_{ij} \cup A_n^i) + I_f(A_{ij} \cup A_n^i; A_p^i)
\end{aligned} \tag{16}$$

Now, we separate each term containing I_f and expand

them based on the definition of SMI in Eq. (5) -

$$\begin{aligned}
I_f(A_{ij}; A_p^i) &= f(A_{ij}) + f(A_p^i) - f(A_{ij} \cup A_p^i) \\
&= \sum_{i,j \in \mathcal{V}} \max_{a \in A_{ij}} S_{ia} + \sum_{i,j \in \mathcal{V}} \max_{p \in A_p^i} S_{ip} \\
&\quad - \sum_{i,j \in \mathcal{V}} \max_{k \in A_{ij} \cup A_p^i} S_{ik} \\
&= \sum_{i,j \in \mathcal{V}} \max_{a \in A_{ij}} S_{ia} + \max_{p \in A_p^i} S_{ip} \\
&\quad - \max \left(\max_{k \in A_{ij}} S_{ik}, \max_{k \in A_p^i} S_{ik} \right) \\
&= \sum_{i,j \in \mathcal{V}} \min \left(\max_{k \in A_{ij}} S_{ik}, \max_{k \in A_p^i} S_{ik} \right)
\end{aligned} \tag{17}$$

Similarly we can calculate $I_f(A_{ij}; A_n^i)$ and $I_f(A_{ij} \cup A_n^i; A_p^i)$ as -

$$I_f(A_{ij}; A_n^i) = \sum_{i,j \in \mathcal{V}} \min \left(\max_{k \in A_{ij}} S_{ik}, \max_{k \in A_n^i} S_{ik} \right) \tag{18}$$

$$I_f(A_{ij} \cup A_n^i; A_p^i) = \sum_{i,j \in \mathcal{V}} \min \left(\max_{k \in A_{ij} \cup A_n^i} S_{ik}, \max_{k \in A_p^i} S_{ik} \right) \tag{19}$$

Substituting these expressions in Eq. (16) and simplifying we get -

$$\begin{aligned}
I_f(A_{ij}; A_n^i | A_p^i) &= H_f(A_{ij} | A_p^i) + H_f(A_{ij} | A_n^i) \\
&\quad - H_f(A_{ij} \cup A_n^i | A_p^i) \\
&= \sum_{i,j \in \mathcal{V}} \max \left(0, \underbrace{\max_{k \in A_{ij}} S_{ik}}_p - \underbrace{\max_{k \in A_p^i} S_{ik}}_r \right) \\
&\quad + \max \left(0, \underbrace{\max_{k \in A_n^i} S_{ik}}_q - \underbrace{\max_{k \in A_p^i} S_{ik}}_r \right) \\
&\quad - \max \left(0, \underbrace{\max_{k \in A_{ij} \cup A_n^i} S_{ik}}_{\text{min}} - \underbrace{\max_{k \in A_p^i} S_{ik}}_r \right)
\end{aligned} \tag{20}$$

This follows the expression $\max(p-r, 0) + \max(q-r, 0) - \max(\max(p, q) - r, 0)$. Which evaluates to -

$$\begin{cases} \max(q-r, 0) & \text{if } p > q, \\ \max(p-r, 0) & \text{if } p < q \end{cases} \tag{21}$$

Thus we can simplify the expression of $I_f(A_{ij}; A_n^i | A_p^i)$ as

$$I_f(A_{ij}; A_n^i | A_p^i) = \sum_{i,j \in \mathcal{V}} \max \left(\min \left(\max_{k \in A_{ij}} S_{ik}, \max_{k \in A_n^i} S_{ik} \right) - \max_{k \in A_p^i} S_{ik}, 0 \right) \tag{22}$$

Substituting this in the expression of $L_{\text{SHASAM}}(\theta)$ we get -

$$L_{\text{SHASAM}}(\theta) = \sum_{i,j \in |\mathcal{V}|} \frac{1}{3|A_{ij}|} \max \left(\min \left(\max_{k \in A_{ij}} S_{ik}, \max_{k \in A_n^i} S_{ik} \right) - \max_{k \in A_p^i} S_{ik}, 0 \right) \dots \text{Hence proved.} \tag{23}$$

□

F.2. SHASAM-LogDetCMI

Given a dataset \mathcal{V} and the Log-Determinant (LogDet) submodular function $f(A) = \text{logdet}(S_A)$ over a set A , we derive a combinatorial loss L_{SHASAM} on the mined anchors A_{ij} , hard positives A_p^i and hard negatives A_n^i based on the Submodular Conditional Mutual Information function $I_f(A_{ij}; A_n^i | A_p^i)$ as shown in Eq. (24).

$$L_{\text{SHASAM}}(\theta) = \sum_{i,j \in |\mathcal{V}|} \frac{1}{3|A_{ij}|} \log \frac{\det(I - S_{A_n^i, A_p^i}^{-1} S_{A_n^i, A_p^i}^T)}{\det(I - S_{A_{ij} \cup A_n^i}^{-1} S_{A_{ij} \cup A_n^i, A_p^i} S_{A_{ij} \cup A_n^i, A_p^i}^T)} \tag{24}$$

Proof. From the definition of CMI based on Mutual Information as described in Eq. (7), we get -

$$\begin{aligned}
I_f(A_{ij}; A_n^i | A_p^i) &= I_f(A_{ij} \cup A_p^i; A_n^i) - I_f(A_n^i; A_p^i) \\
&= f(A_{ij} \cup A_p^i) + f(A_n^i) - f(A_{ij} \cup A_p^i \cup A_n^i) \\
&\quad - f(A_n^i) + f(A_p^i) - f(A_n^i \cup A_p^i)
\end{aligned} \tag{25}$$

Given the definition of LogDet over a set A , $f(A) = \text{logdet}(S_A)$, we substitute this in the above equation to get the following -

$$\begin{aligned}
I_f(A_{ij}; A_n^i | A_p^i) &= \text{logdet}(S_{A_{ij} \cup A_p^i}) + \text{logdet}(S_{A_n^i}) \\
&\quad - \text{logdet}(S_{(A_{ij} \cup A_p^i) \cup A_n^i}) \\
&\quad - \text{logdet}(S_{A_n^i}) + \text{logdet}(S_{A_p^i}) \\
&\quad - \text{logdet}(S_{A_n^i \cup A_p^i}) \\
&= \log \left(\frac{\det(S_{A_{ij} \cup A_p^i}) \cdot \det(S_{A_n^i})}{\det(S_{A_{ij} \cup A_p^i \cup A_n^i})} \right) \\
&\quad - \log \left(\frac{\det(S_{A_n^i}) \cdot \det(S_{A_p^i})}{\det(S_{A_n^i \cup A_p^i})} \right)
\end{aligned} \tag{26}$$

From Schur's complement we know that $\det(S_{A \cup B}) = \det(S_A)\det(S_{A \cup B} \setminus S_A)$ and $S_{A \cup B} \setminus S_A = S_B - S_{A,B}^T S_A^{-1} S_{A,B}$, where $S_{A,B}$ refers to the cross-similarities between sets A and B while S_A and S_B represent the corresponding self-similarities. We use this to simplify the expression of I_f above as follows -

$$\begin{aligned}
I_f(A_{ij}; A_n^i | A_p^i) &= \log \left(\frac{\det(A_n^i)}{\det(S_{A_{ij} \cup A_p^i \cup A_n^i} \setminus S_{A_{ij} \cup A_p^i})} \right) \\
&\quad - \log \left(\frac{\det(S_{A_p^i})}{\det(S_{A_n^i \cup A_p^i} \setminus S_{A_n^i})} \right) \\
&= \log \det \left(\frac{S_{A_n^i \cup A_p^i} \setminus S_{A_n^i}}{S_{A_p^i}} \right) \\
&\quad - \log \det \left(\frac{S_{A_{ij} \cup A_p^i \cup A_n^i} \setminus S_{A_{ij} \cup A_p^i}}{S_{A_n^i}} \right) \\
I_f(A_{ij}; A_n^i | A_p^i) &= \log \det \left(\frac{S_{A_p^i} - S_{A_{ij}^T, A_p^i}^T S_{A_n^i}^{-1} S_{A_n^i, A_p^i}}{S_{A_p^i}} \right) \\
&\quad - \log \det \left(\frac{S_{A_n^i} - S_{A_{ij} \cup A_p^i, A_n^i}^T S_{A_{ij} \cup A_p^i}^{-1} S_{A_{ij} \cup A_p^i, A_n^i}}{S_{A_n^i}} \right) \\
&= \log \det \left(I - S_{A_p^i}^{-1} S_{A_n^i, A_p^i}^T S_{A_n^i}^{-1} S_{A_n^i, A_p^i} \right) \\
&\quad - \log \det \left(I - S_{A_n^i}^{-1} S_{A_{ij} \cup A_p^i, A_n^i}^T S_{A_{ij} \cup A_p^i}^{-1} S_{A_{ij} \cup A_p^i, A_n^i} \right) \tag{27}
\end{aligned}$$

Following simple logarithmic principles we can further simplify this expression as -

$$I_f(A_{ij}; A_n^i | A_p^i) = \log \frac{\det(I - S_{A_n^i}^{-1} S_{A_n^i, A_p^i}^T S_{A_n^i}^{-1} S_{A_n^i, A_p^i}^T)}{\det(I - S_{A_{ij} \cup A_p^i}^{-1} S_{A_{ij} \cup A_p^i, A_n^i}^T S_{A_{ij} \cup A_p^i}^{-1} S_{A_{ij} \cup A_p^i, A_n^i}^T)} \tag{28}$$

Substituting this in the equation of $L_{\text{SHASAM}}(\theta)$ in Eq. (14) we get the loss function for SHASAM-LogDetCMI as shown below.

$$L_{\text{SHASAM}}(\theta) = \sum_{i,j \in |\mathcal{V}|} \frac{1}{3|A_{ij}|} \log \frac{\det(I - S_{A_n^i}^{-1} S_{A_n^i, A_p^i}^T S_{A_n^i}^{-1} S_{A_n^i, A_p^i}^T)}{\det(I - S_{A_{ij} \cup A_p^i}^{-1} S_{A_{ij} \cup A_p^i, A_n^i}^T S_{A_{ij} \cup A_p^i}^{-1} S_{A_{ij} \cup A_p^i, A_n^i}^T)} \tag{29}$$

Table 5. **Ablation on selection budget in SHASAM** measured in terms of Top-1 Accuracy (Acc.) and equalized odds (EO) by varying the budget k on two settings in CelebA dataset. The learning objective was kept constant at SHASAM-LEARN w/ FLCMI and the selection strategy in SHASAM-MINE is set to FLCMI.

| Selection Strategy | Budget k | $T = a / S = m$ | | $T = a / S = y$ | |
|--------------------|------------|-----------------|----------|-----------------|----------|
| | | EO (↓) | Acc. (↑) | EO (↓) | Acc. (↑) |
| FSCL [48] | - | 6.5 | 79.1 | 12.4 | 79.1 |
| SHASAM | 8 | 7.0 | 79.9 | 10.2 | 77.2 |
| SHASAM | 16 | 5.6 | 81.3 | 9.9 | 79.58 |
| SHASAM | 24 | 5.5 | 81.08 | 10.1 | 79.44 |

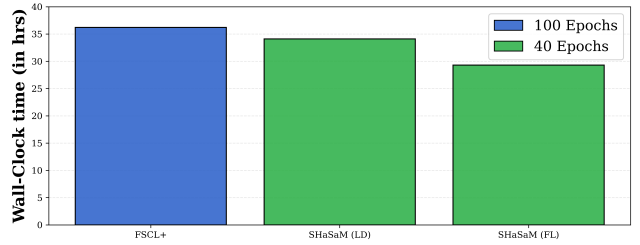


Figure 6. **Ablation on Computational Cost** measured in terms of wall clock time averaged over three settings in CelebA dataset. The submodular function in the learning objective and selection strategy in SHASAM was kept constant.

For performance, we utilize **Balanced Accuracy** (BA), a metric particularly effective for datasets with imbalanced class distributions. Rather than a simple accuracy score, BA calculates the average of the true positive and true negative rates across each subgroup, offering a more nuanced view of a model's effectiveness and ensuring that high performance on a majority group does not obscure poor performance on a minority group.

For fairness, we employ two widely accepted metrics. The first, **Demographic Parity** (DP), measures whether the rate of positive predictions is consistent across different sensitive groups. A model satisfies DP if its decisions are statistically independent of an individual's group membership, with a value approaching zero indicating greater fairness.

The second metric, **Equalized Opportunity** (EOpp), enforces a more stringent fairness condition by requiring that the model's true positive rate is the same for all sensitive groups. This ensures the model is equally effective at correctly identifying positive instances, regardless of group identity. For both DP and EOpp, scores closer to zero signify a more equitable model.

G. Additional Fairness Metrics (Contd. from Sec. 4)

To provide a comprehensive evaluation of our model, we assess both its predictive performance and its adherence to fairness principles. In addition the reported metrics in Sec. 4 of the main paper we also evaluate our model on additional metrics that have been used in SoTA approaches.

H. Additional Results

H.1. Additional Results from Metrics in Appendix G

Although Equalized Odds is the most commonly adopted fairness metric in literature there exists metrics such as Demographic Parity (DP), Equalized Opportunity (EOpp)

Table 6. A comparison of different methods across three distinct tasks. The tasks involve predicting an attribute (T) while maintaining fairness with respect to a sensitive attribute (S). We report Accuracy (Acc.), Balanced Accuracy (BA), Equalized Opportunity (EOpp.), and Demographic Parity (DP). Higher ACC and BA are better, while lower EO and DP are better. The best result in each column is highlighted in bold.

| method | $T = a / S = m$ | | | | $T = s / S = m$ | | | | $T = a / S = br$ | | | |
|------------------------------|-----------------|--------------|----------------|--------------|-----------------|--------------|----------------|--------------|------------------|--------------|----------------|--------------|
| | Acc.% | BA% | EOpp. $_{e-2}$ | DP $_{e-1}$ | Acc.% | BA% | EOpp. $_{e-2}$ | DP $_{e-1}$ | Acc.% | BA% | EOpp. $_{e-2}$ | DP $_{e-1}$ |
| Vanilla | 74.01 | 72.36 | 14.43 | 3.245 | 88.42 | 88.85 | 4.91 | 1.489 | 76.48 | 74.55 | 3.61 | 1.896 |
| TADeT-MMD [52] | 79.89 | 73.85 | 7.10 | 3.693 | 92.51 | 93.03 | 2.48 | 1.290 | 77.97 | 75.64 | 2.27 | 1.491 |
| TADeT [52] | 78.73 | 74.52 | 3.11 | 3.116 | 90.05 | 90.68 | 4.86 | 1.443 | 78.49 | 77.42 | 3.78 | 1.057 |
| FSCL [48] | 79.09 | 74.76 | 1.78 | 3.004 | 89.37 | 90.08 | 1.76 | 1.344 | 78.85 | 78.06 | 2.65 | 0.989 |
| FSCL+ [48] | 77.26 | 73.42 | 0.79 | 2.604 | 88.83 | 89.02 | 1.20 | 1.263 | 78.02 | 77.37 | 1.79 | 0.834 |
| FairViT [63] | 83.80 | 79.96 | 1.15 | 2.837 | 94.27 | 94.12 | 1.52 | 1.205 | 82.52 | 81.56 | 2.10 | 0.701 |
| SHASAM(w/ FLCMI, ViT) (ours) | 84.01 | 80.16 | 0.76 | 2.582 | 92.87 | 94.57 | 1.17 | 1.193 | 80.70 | 79.42 | 2.06 | 0.873 |

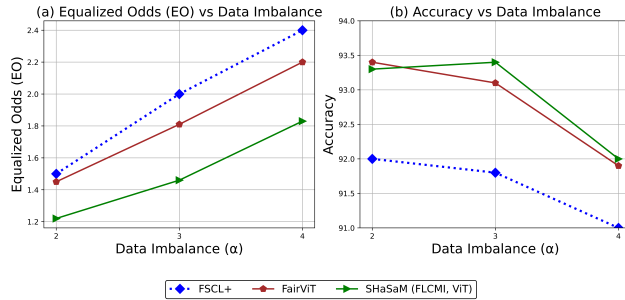


Figure 7. **Results of SHASAM on UTKFace dataset on ViT-based benchmark** (FairViT) measuring (a) Equalized Odds and (b) Top-1 Acc. under varying inter-group imbalance (α). The target and sensitive attributes are set to *gender* and *ethnicity* respectively following setup in Park et al. [48].

and Balanced Accuracy (BA) that are studied in the context of fair facial attribute recognition. In addition to Equalized Odds (EO) in Tab. 2 (main paper) we present results from the aforementioned metrics by closely following the exact benchmark in FairViT [63] in Tab. 6. Similar to FairViT we also adopt three distinct settings by varying T and S - $T =$ attractiveness (a) / $S =$ gender (male, m), $T =$ expression (smiling, s) / $S =$ gender (male, m), $T =$ attractiveness (a) / $S =$ hair-color (brown, br). Similar to our observations in Tab. 2 (main paper) we see that SHASAM (with FLCMI as the instance for SHASAM-MINE and SHASAM-LEARN) achieves competitive accuracy (indicated as Acc.) to FairViT without the requirement to train the Vision Transformer (ViT) architecture from scratch. Finally, the self-balancing property as elucidated in [42] ensures that majority classes do not bias the decisions made by SHASAM. This is reflected in the boost in performance measured through BA across all downstream tasks.

H.2. Comparison against FairViT on UTKFace Dataset

In continuation to the results presented in Sec. 4.1 on UTKFace dataset we include experiments contrasting the performance of SHASAM against FairViT [63]. For fair comparisons we replace the resnet based backbone in SHASAM

with a ViT based backbone and depicts the results in Fig. 7 under similar imbalanced settings discussed in Sec. 4.1 and report the top-1 accuracy and EO through Fig. 7(b) and Fig. 7(a). Similar to Sec. 4.1 we show that our SHASAM w/ FLCMI approach shows improvements in both EO and accuracy under varying degrees of imbalance.

H.3. Ablation on the selection Budget

As discussed in Sec. 4 of the main paper, SHASAM learns from a set of mined anchors, hard-positives and hard-negatives. Since the selection of exemplars in each of these sets is performed through submodular optimization under the knapsack constraint [45], a fixed budget k is established for each set. For simplicity we keep this budget constant across three sets discussed above such that in each iteration there are exactly k anchors, k hard-positives and k hard-negatives resulting in a total batch size of $3k$ (excluding augmentations). From the results tabulated in Tab. 5 a pattern emerges wherein a higher budget (more examples) benefit both fairness and accuracy metrics. However, its interesting to note that the performance saturates beyond $k = 16$. Due to this (alongside compute limitations) we adopt a selection budget of 16 in all our experiments. Note, we were unable to execute experiments with higher selection budgets in Tab. 5 due to compute limitations.

H.4. Ablation: Choice of Combinatorial Function in SHASAM

As discussed in Sec. 3.4 and 3.5 the choice of submodular function f induces various combinatorial properties encoded in SHASAM-MINE and SHASAM-LEARN. In Tab. 3 of the main paper we vary the submodular function between LD (indicating LogDetCMI) and FL (indicating FLCMI) functions and report the performance both in terms of EO and accuracy (indicated as Acc. in Tab. 3). At first, we show that FL based selection and learning functions demonstrate improved performance and fairness. This is because Facility-Location (the submodular function in these instances) models representation in contrast to diversity (modeled by LogDet), mining representative anchors,

positives and negatives in SHASAM-MINE while learning representative features in SHASAM-LEARN.

H.5. Ablation: Compute Cost and Wall Clock time

We point out that introduction of the learning formulation in SHASAM does not add any additional parameters to the model. Nevertheless, particular instances of SHASAM like LogDetCMI requires computation of large matrices which scale with the increase in batch size requiring large compute infrastructure. We have discussed this in the limitations of our paper in Appendix I.

Additionally, we also compare the wall-clock time requirements of SHASAM against SoTA methods in Fig. 6. For each setting in Fig. 6 we calculate the average time in phase 1 (phase 2 remains largely unchanged) across three distinct settings in CelebA. Our observations closely follow the discussion in Sec. 4.2 (main paper) which shows that adopting a combinatorial approach in SHASAM requires fewer training epochs in stage 1 (100 epochs in FSCL to ~ 40 epochs in SHASAM). However, the selection of hard positives and negatives do add a computation overhead which reflects in the wall-clock times shown in Fig. 6. This has been listed as a limitation in Appendix I.

H.6. Characterization of SHASAM-MINE on Synthetic Data

To characterize the effectiveness of the introduced SHASAM-MINE we simulate three different scenarios. These include variation in sample sizes between target attributes inducing *imbalance* and simulating *feature overlap* between groups inducing inter-group bias. Our goal is to show that minimizing L_{SHASAM} on the mined anchors, hard positives and negatives facilitate the learning of strong decision boundaries between target attributes while ensuring learning of compact feature clusters (minimize intra-group variance) for each target attribute label without biasing on the sensitive attribute labels.

Balanced Settings In this case both clusters A and B as shown in Fig. 8 have equal number of samples with distinguishable decision boundary between them. In contrast to *Random* selection which is the most widely used technique, SHASAM-MINE selects diverse anchors representing the complete target set (in this case cluster B). Additionally, our approach selects hard-positives which lie at the cluster boundary of B . Minimizing the separation between these hard-positives and anchors result in minimization of intra-group variance encouraging the model to be unbiased to the sensitive attributes. Lastly, hard-negatives in A also lie at the cluster boundary between A and B , resulting in increased decision boundary when the separation between hard-positives and and negatives are maximized through L_{SHASAM} .

Imbalanced Settings In this case clusters A and B as

shown in Fig. 9 demonstrate imbalance with A being the rare group, with distinguishable decision boundary between them. Alongside selection of diverse anchors, SHASAM-MINE selects hard-positives and negatives which continue to lie at the cluster boundary of A and B irrespective of the choice of target attribute label (anchors are mined from this set) - Rare class A in Fig. 9 and abundant class B in Fig. 4 of main paper. Minimizing L_{SHASAM} over the mined sets promotes reduction in intra-group variance within the groups and maximizes inter-group separation between the target attribute and the remaining groups encouraging the model to learn features, unbiased to the sensitive attributes. **Feature Similarity (Cluster Overlap)** In contrast to distinct cluster boundaries depicted in Fig. 8 and Fig. 9 we introduce a case with high inter-group bias demonstrated as overlapping feature clusters A and B in an imbalanced setting (B being the abundant and A being the rare group). The behavior of SHASAM-MINE is consistent with the previous setting and mines hard positives and negatives at the cluster boundary. Interestingly, we see that SHASAM-MINE selects hard-negatives that largely represent the overlapped section of the embedding space which when consumed by L_{SHASAM} would promote mitigation of inter-group bias and enforce strong decision boundaries between target attributes.

H.7. Standard Deviation of Results on CelebA

We indicate in Section 4.1 of the main paper that we report the average performance over three independent runs by varying the seed value of underlying libraries among three random seeds. We supplement the results in Table 2 with standard deviation numbers in Tab. 7 for SHASAM variants and methods which were re-implemented by us. We show that models trained with SHASAM achieves the lowest standard deviations among all compared approaches. This can be attributed to the combinatorial formulation which allows the model to learn from complete sets of anchors, positives and negatives rather than contrasting individual samples [63] or one anchor pair and multiple positives and negatives [48].

I. Limitations

While the SHASAM framework presents a novel combinatorial approach for fair facial attribute recognition, it has a few limitations. The primary constraint is the computational cost and wall-clock time overhead associated with the SHASAM-MINE stage, which involves combining submodular optimization and representation learning in a unified framework. To remedy this, SHASAM relies on training with a randomly selected subset of the dataset at each epoch, which could be inefficient for extremely large-scale applications. Further, SHASAM operates on the assumption that discrete target and sensitive attributes are available,

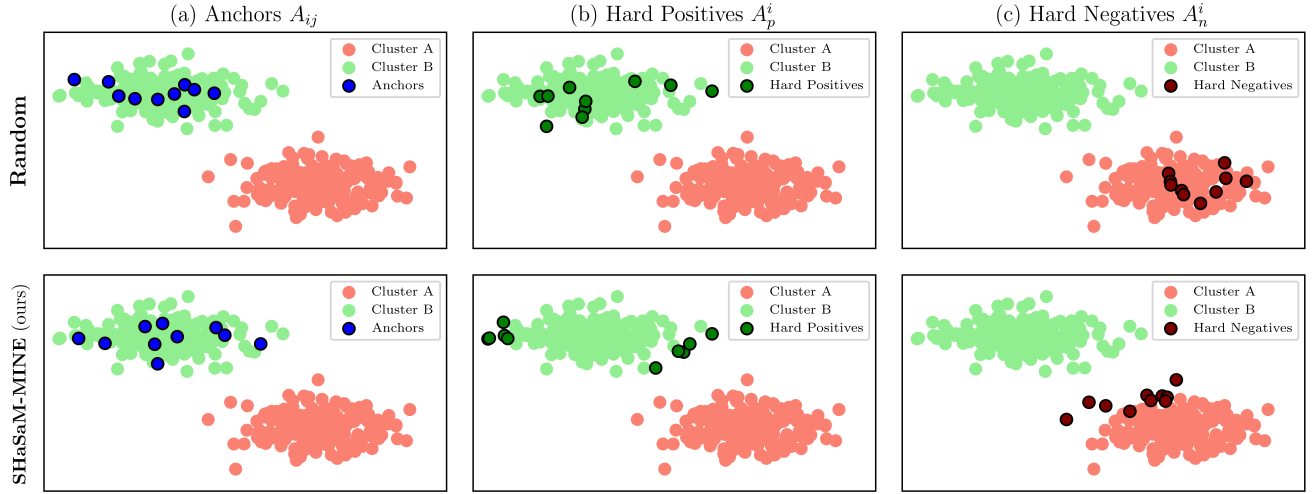


Figure 8. **Contrasting Random and SHASAM-MINE selection strategies** on a synthetic two-cluster imbalanced dataset to identify (a) Anchors, (b) Hard Positives and (c) Hard Negatives, in the *balanced* setting. The dataset generation and sample selection in performed under the same seed.

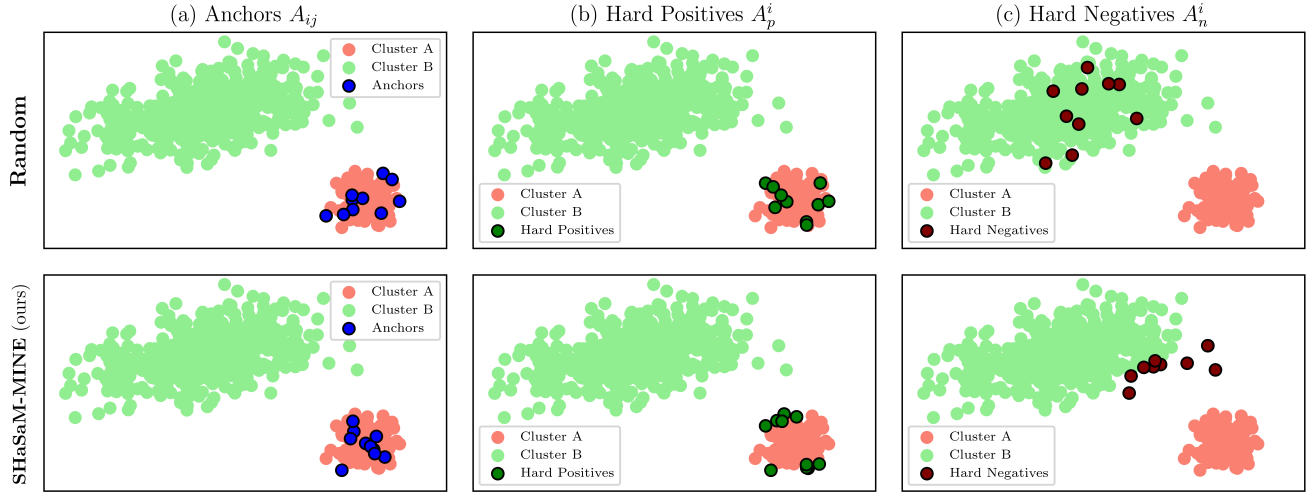


Figure 9. **Contrasting Random and SHASAM-MINE selection strategies** on a synthetic two-cluster imbalanced dataset with target attribute as the minority (rare) class. SHASAM-MINE identifies (a) Anchors, (b) Hard Positives and (c) Hard Negatives, showing the effectiveness of SHASAM in modeling the decision boundary between target attributes. The dataset generation and sample selection in performed under the same seed.

and in experiments, continuous attributes like 'age' were simplified into binary categories, a step that may not be suitable for all real-world scenarios. Finally, complex sub-modular functions like Log-Determinant may require computing large matrices (given a large batch size) which might expand the compute requirements beyond the available budget.

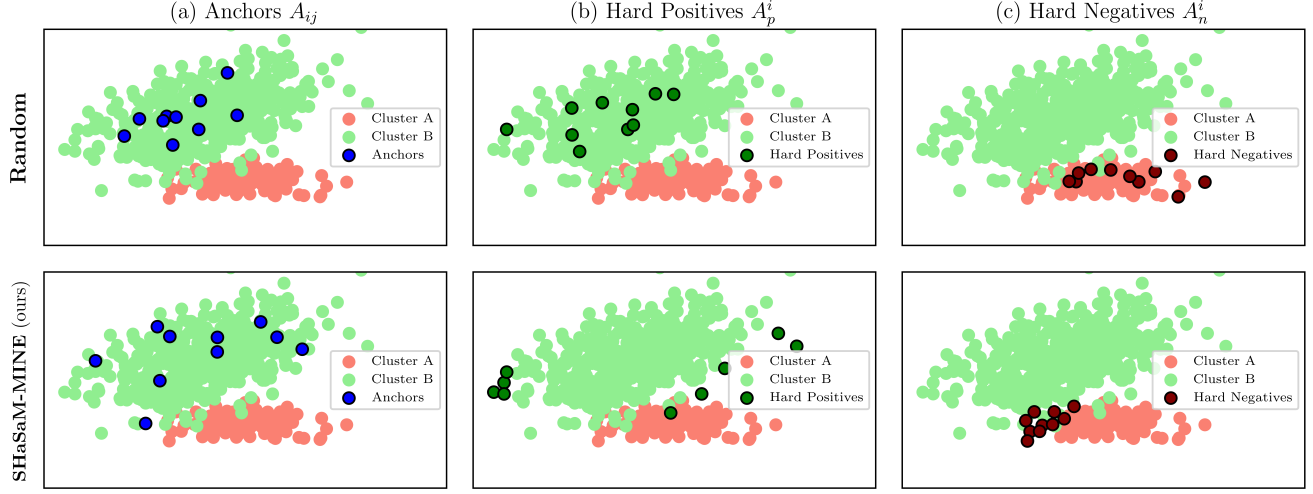


Figure 10. **Contrasting Random and SHaSAM-MINE selection strategies** on a synthetic two-cluster imbalanced dataset to identify (a) Anchors, (b) Hard Positives and (c) Hard Negatives, when large feature similarity exists between clusters (overlapping clusters). The dataset generation and sample selection in performed under the same seed.

Table 7. **Classification results with standard deviations on CelebA** measured in terms of Top-1 Accuracy (Acc.) and equalized odds (EO) by varying the target T and sensitive attributes S . Here, a , b , e , m , and y denote attractiveness, big nose, bags-under-eyes, male, and young, respectively. All results are averaged over three independent runs. * indicates our re-implementations. All values are rounded off to 1 decimal point.

| Method | $T = a / S = m$ EO (↓) Acc. (↑) | $T = a / S = y$ EO (↓) Acc. (↑) | $T = b / S = m$ EO (↓) Acc. (↑) | $T = b / S = y$ EO (↓) Acc. (↑) | $T = e / S = m$ EO (↓) Acc. (↑) | $T = e / S = y$ EO (↓) Acc. (↑) | $T = e \& b / S = m$ EO (↓) Acc. (↑) | $T = a / S = m \& y$ EO (↓) Acc. (↑) |
|----------------------------|------------------------------------|------------------------------------|------------------------------------|------------------------------------|------------------------------------|------------------------------------|---|---|
| CE [2] | 27.8 ±0.4 | 79.6 ±0.4 | 16.8 ±0.5 | 79.8 ±0.5 | 17.6 ±0.3 | 84.0 ±0.5 | 14.7 ±0.3 | 84.5 ±0.5 |
| GRL [51] | 24.9 ±0.3 | 77.2 ±0.3 | 14.7 ±0.5 | 74.6 ±0.5 | 14.0 ±0.4 | 82.5 ±0.4 | 10.0 ±0.3 | 83.3 ±0.5 |
| LNL [34] | 21.8 ±0.2 | 79.9 ±0.3 | 13.7 ±0.5 | 74.3 ±0.5 | 10.7 ±0.6 | 82.3 ±0.6 | 6.8 ±0.3 | 82.3 ±0.6 |
| FD-VAE [47] | 15.1 ±0.2 | 76.9 ±0.3 | 14.8 ±0.5 | 77.5 ±0.5 | 11.2 ±0.4 | 81.6 ±0.4 | 6.7 ±0.3 | 81.7 ±0.4 |
| MFD [25] | 7.4 ±0.1 | 78.0 ±0.2 | 14.9 ±0.4 | 80.0 ±0.4 | 7.3 ±0.3 | 78.0 ±0.3 | 5.4 ±0.2 | 78.0 ±0.3 |
| SupCon [31] | 30.5 ±0.3 | 80.5 ±0.4 | 21.7 ±0.7 | 80.1 ±0.7 | 20.7 ±0.6 | 84.6 ±0.4 | 16.9 ±0.5 | 84.4 ±0.3 |
| FSCL (w/ group norm) [48]* | 6.5 ±0.4 | 79.1 ±0.4 | 12.4 ±0.5 | 79.1 ±0.5 | 4.7 ±0.5 | 82.9 ±0.4 | 4.8 ±0.3 | 84.1 ±0.5 |
| SHaSAM(w/ LogDetCMI) | 6.1 ±0.2 | 80.7 ±0.3 | 10.5 ±0.5 | 78.6 ±0.5 | 3.6 ±0.6 | 84.5 ±0.2 | 4.2 ±0.3 | 85.9 ±0.3 |
| SHaSAM(w/ FLCMI) | 5.5 ±0.3 | 81.3 ±0.4 | 9.9 ±0.7 | 79.6 ±0.7 | 3.3 ±0.6 | 84.7 ±0.4 | 3.9 ±0.5 | 87.0 ±0.3 |
| FSCL (w/ ViT) [48] | 5.7 ±0.4 | 79.9 ±0.2 | 10.8 ±0.5 | 80.0 ±0.3 | 4.0 ±0.3 | 85.0 ±0.4 | 4.6 ±0.4 | 88.2 ±0.6 |
| FairViT [63]* | 6.4 ±0.2 | 83.8 ±0.4 | 12.6 ±0.2 | 82.5 ±0.1 | 5.1 ±0.4 | 86.1 ±0.1 | 4.7 ±0.2 | 89.3 ±0.1 |
| SHaSAM(w/ FLCMI, ViT) | 5.3 ±0.2 | 84.0 ±0.3 | 9.9 ±0.4 | 82.3 ±0.1 | 3.0 ±0.3 | 85.6 ±0.2 | 3.7 ±0.2 | 89.2 ±0.2 |